ACS OMEGA

Open Access

http://pubs.acs.org/journal/acsodf

Article

Curcumin-Conjugated PAMAM Dendrimers of Two Generations: Comparative Analysis of Physiochemical Properties Using Adriatic Topological Indices

Anuradha D. S., Konsalraj Julietraja, B. Jaganathan, and Ammar Alsinai*

Cite This: *ACS Omega* 2024, 9, 14558−14579

Read Online

ACCESS | Metrics & More | Article Recommendations | Supporting Information

ABSTRACT: Curcumin ($C_{21}H_{20}O_6$) is a polyphenol found in the plant *Curcuma longa*. Even though it possesses many pharmacological effects, owing to its limited intestinal absorption, solubility, and oral bioavailability, it is more often used as a health supplement than as a lead chemical. The poly(amido)amine (PAMAM) dendrimer (nanostructure) is utilized to enhance the stability and targeted delivery of drugs. Recently, curcumin was conjugated with the PAMAM dendrimer and analyzed for its photostability. Further investigation into the physiochemical characteristics of different generations can facilitate curcumins' targeted delivery for many diseases, including cancer. However, many of these conjugates' physiochemical properties are not available in databases since they have not been explored theoretically or experimentally. In this article, QSAR/QSPR (quantitative structure−activity relationship/quantitative structure−property relationship) analysis of physiochemical properties was carried out for component structures, which produced encouraging results. Hence, 16 discrete adriatic topological indices and their associated entropy measures were evaluated to theoretically predict a few physiochemical properties of the conjugated structure. The predictions will aid the chemist in drug designing.

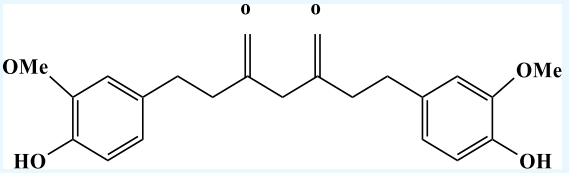

1. INTRODUCTION

Curcumin, a polyphenol isolated from the perennial plant *Curcuma longa* in 1815, possesses a symmetric molecular structure ($C_{21}H_{20}O_6$) depicted in Figure 1 and has a molecular weight of 368.38. The IUPAC name of curcumin is (1*E*,6*E*)-1,7-bis (4-hydroxy-3-methoxyphenyl)-1,6-heptadiene-3,5-dione.[1]

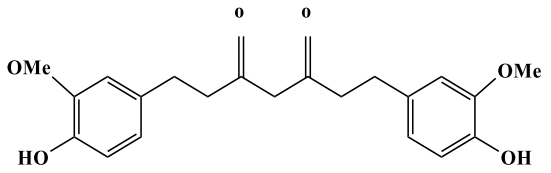

Figure 1. Residue R_1—molecular structure of curcumin residue.

Curcumin possesses abundant pharmacologic properties and are used as anti-inflammatory,[2] antioxidant,[3] antimicrobial,[4] anti-HIV,[5] antifungal,[6] antibacterial,[7] antiviral,[8] antitumoral,[9] anticancer, antiamyloid,[10] anti-Alzheimers agents,[10] and so on.[11] It also acts as an immune modulator, metabolism regulator, neuroprotector,[12] and tissue protector.[2] It has a wide range of applications apart from dietary supplements, namely, in the food industry (colorant and preservative), cosmetics manufacturing,[13] and textile manufacturing (dyeing).[14]

However, curcumin's limited absorption in the stomach leads to nonsignificant levels in the bloodstream which affects its wide usage as a lead compound.[15] This is because of its poor oral bioavailability, poor solubility, and hydrophobicity.[16] A study of literature based on biological investigations, including patients, healthy individuals, laboratory animals, and human cells, concluded that further theoretical and experimental research is required to fully utilize the medical benefits of curcumin.[17,18]

Nowadays, medical research is focusing on certain incurable diseases affecting the skin, lungs, tumors, and other internal organs. Brain tumor, cancer, and genetic disorders are some of incurable diseases that are treated and managed only on a day-to-day basis.[19] Once the pharmacological property of curcumin is improved, it may be used as a therapy for illnesses, including cancer, COVID-19, and so on.

Numerous strategies have been used to increase curcumin's bioavailability. These methods include the use of piperine (present in black pepper), nanoparticles, and liposomes.[18] Even the conjugates that are considered as appropriate curcumin transporters have shown constrained, unreliable, and inconsistent results in clinical studies[20,21]

1.1. PAMAM Dendrimers.

Dendrimers are one among the nanostructures that possess tenable sizes and branch compositions,[22] which help to tackle the difficulties in solubility, stability,

Received: January 21, 2024
Revised: February 20, 2024
Accepted: February 26, 2024
Published: March 12, 2024

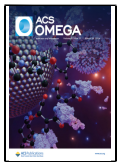

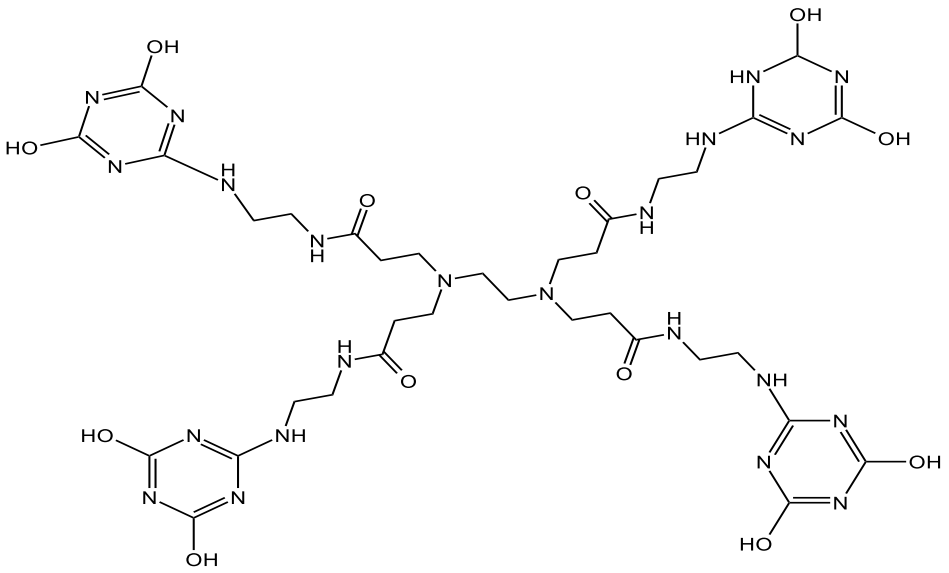

Figure 2. Core of PAMAM dendrimer first generation.

Table 1. Physiochemical Properties Taken from ChemSpider

s. no.	physiochemical properties	curcumin	PAMAM dendrimer first generation
1	molar volume	287.9	444.6
2	enthalpy of vaporization	91.5	131.2
3	density	1.3	1.2
4	Log *P*	2.92	−5.83
5	refraction index	104	1.543
6	vapor pressure	1.7	0
7	surface tension	54.3	54.3
8	polarizability	41.2	55.5
9	flash point	208.9	499.3
10	boiling point	591.4	902

and bioavailability,[23,24] and hence regarded as a breakthrough in nanosized bioactive delivery mechanisms. PAMAM dendrimers are one among the five main types of identified dendrimers, and each class differs from the others in terms of its process of synthesis, base core, structural behavior, and terminal groups. They are nanoformulations which act as a nanocarrier for bioactive chemicals to address problems with solubility, stability, and bioavailability.[25]

"PAMAM" stands for Poly(AMido)AMine which refers to dendrimer types built by polyamide branches with tertiary amines as focal points and has potential usage in improving the solubility of drug delivery systems.[26]

They are possibly the oldest complete dendrimer family grown using two reaction stages and divergent layer-by-layer (inside-out) development.[27] The molecular structure of PAMAM dendrimer used as the core for developing the conjugation is depicted in Figure 2.

One popular method in the ligand-based drug design process is quantitative structure−activity relationship/quantitative structure−property relationship (QSAR/QSPR). This is used to predict and optimize current leads and enhance their biological activities and physiochemical characteristics of untested and unavailable substances.[28−30] Three kinds of dendrimer networks,[31] biconjugate networks,[32] nanostructures of cerium oxide,[33] and Sudoku nanosheets,[34] are analyzed using topological indices (TIs).

1.2. QSAR/QSPR Analysis. Correlations between the biological activities of substances and their analogues are derived through QSAR/QSPR. The mathematical regression methods are widely used in pharmacodynamics, chemometrics, toxicology, and pharmacokinetics.[35] Several TIs are defined for hypoglycemic agents, anti-Alzheimers drugs, antiparasitic drugs, headache medications, and cancer medications to aid researchers in understanding their physical properties and related chemical processes.[36−40]

The conjugated structures' physiochemical properties are not available in globally recognized databases. Hence, QSAR/QSPR analysis is performed for individual structures by using data available in ChemSpider.

Randomly chosen discrete adriatic TIs (explained in Section 4.5) are utilized to evaluate the physiochemical properties of individual molecular structures that were employed to form conjugates: curcumin and PAMAM dendrimer first generation. The physiochemical properties taken from ChemSpider are listed in Table 1.

The ten randomly selected numerical values of discrete adriatic TIs calculated for curcumin (Figure 1) and PAMAM dendrimer first generation (Figure 2) are enumerated in Table 2.

The correlation coefficient values obtained for the chemical structure and its corresponding TIs were **0.92243** and **0.91698**. These promising results enable further linear regression analysis. The correlation coefficient (r) expresses the level of predictability of the relationship, the model's fit, and the degree

https://doi.org/10.1021/acsomega.4c00686
ACS Omega 2024, 9, 14558−14579

Table 2. TIs of Curcumin and PAMAM Dendrimer First Generation

s. no	TIs	curcumin	PAMAM dendrimer first generation
1	SLI	43.3038	281.0548
2	ISLI	28.3	178.8
3	MLSI	−2.9342	113.4256
4	MII	6.3333	34.33333
5	MIRI	4.412	24.034
6	MRI	−8.844	50.388
7	MMRI	20.877776	137.91648
8	MMDI	8	270
9	SDDI	62.3333	387
10	MMSDI	91.5	508.5

of variance in the data. The squared correlation coefficient, or r^2, is used to determine how repeatable the model's experimental data is.[41] The statistical parameters derived from the linear regression are given in Table 3.

Table 3. Statistical Parameters Obtained from Linear Regression Analysis

	chemical structure	
statistical parameter	curcumin	PAMAMfirst generation
no. of observations	10	10
correlation coefficient (r)	0.92243	0.91698
r^2	0.850879	0.840859
F-statistics	45.648	42.2699
significance level (p)	0.0001	0.0001
A	5.3498	1.7466
B	3.0115	−138.4

For better interpretation, the linear regression is presented graphically in Figures 3 and 4.

The statistical significance and precision of the chemical activity prediction are key factors in QSAR model reliability. A dependable QSAR/QSPR model of best fit is determined by statistical data, an r value closer to 1, and r^2 of at least 0.6, and a significance level less than 0.05.[42] From Table 3, it is evident that both of the molecular structures exhibit a good significance level and a strong correlation. The relevance and optimal fit of the linear regression models are confirmed by each of the statistical parameters mentioned above. The TIs under examination and the physicochemical characteristics of the compounds under exploration show a strong correlation in this QSPR model.

1.3. Necessity for Further Investigation. When curcumin's bioavailability is increased, it can be used to treat dermatological conditions, suppress the growth of tumors, treat HIV and cancer, and regulate the immune system and metabolism.[43] Researchers have synthesized and investigated the photostability of curcumin conjugated with PAMAM dendrimers.[44,45] An analysis of different generations of these conjugates must also be explored. However, the investigation of physiochemical characteristics and the comparative analysis of different generations demand time, labor, and experimental costs. To overcome these difficulties, this article attempts to predict a few physiochemical properties related to drug designing theoretically. The comparative analysis of the first and second generations is also presented graphically along with the predictions.

The main factors that are crucial at every step of drug discovery and development are mainly determined by the drug-likeness filters. These are based on physiochemical properties, namely water partition coefficient (octanol), molecular weight, vaporization, enthalpy of vaporization, retention time, biological activity, etc. which speed up the process of drug development.[46,47]

Discrete adriatic TIs exhibit strong correlations to physiochemical parameters, namely octanol−water partition coefficient (Log P), heat capacity, biological activity, total surface area, enthalpy of vaporization, standard enthalpy of vaporization, and relative retention time.[48−50] In this regard, discrete adriatic TIs and their respective entropy measures are calculated for first- and second-generation curcumin-conjugated PAMAM dendrimers. A comparative analysis of these generations is presented graphically. Curcumin conjugated with PAMAM dendrimers has not yet been studied theoretically through any TIs. Since the research is still evolving, the theoretical predictions made through discrete adriatic TIs may be used for potential applications.[49]

2. CURCUMIN-CONJUGATED PAMAM DENDRIMERS

When PAMAM dendrimers are combined with curcumin, van der Waals forces, interactions with hydrophobic molecules, and hydrogen bonds help to retain the conjugated structure of the compound.[51] The behavior of the interface among curcumin and PAMAM dendrimers was studied using UV spectroscopy, molecular model, and fluorescence methods.[52] To improve curcumin's oral bioavailability, PAMAM fourth-generation dendrimers conjugated with curcumin were developed. This promoted absorption in the gastrointestinal tract and sustained therapeutic medication administration.[53] The glioblastoma (a fatal and aggressive tumor) cell line viability was specifically decreased by curcumin-loaded dendrimers. Utilizing and improving PAMAM dendrimer conjugates offer a promising

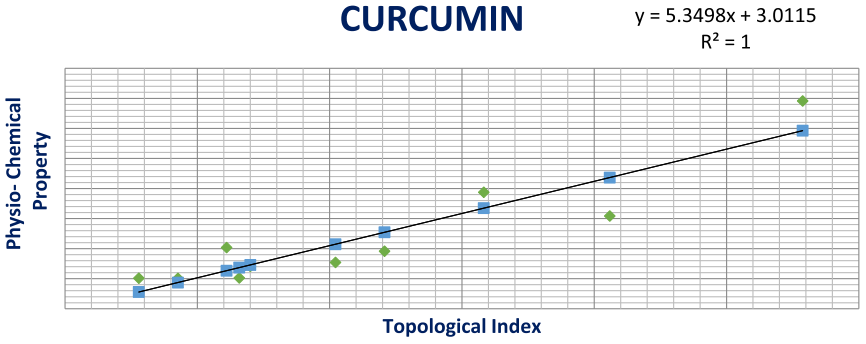

Figure 3. Linear regression plots for curcumin.

https://doi.org/10.1021/acsomega.4c00686
ACS Omega 2024, 9, 14558−14579

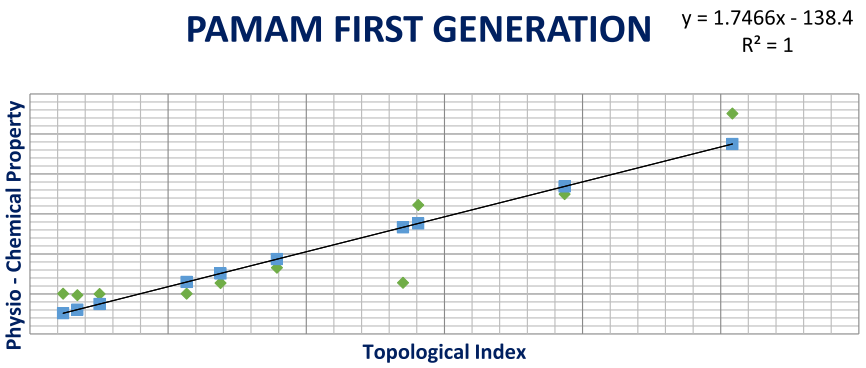

Figure 4. Linear regression plots for PAMAM dendrimer first generation.

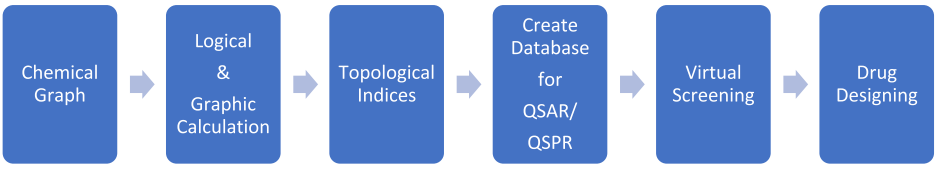

Figure 5. Workflow from molecular structure to drug designing.

new method of delivering cancer therapies. The outcomes also revealed that curcumin antioxidants are effective in glioblastoma treatment.[12]

In the forthcoming section, some of the key information necessary to understand conjugation and discrete adriatic TIs-associated physiochemical properties is briefly explained. The analytical formula for the molecular structure of the first and second generations of adriatic discrete TIs of curcumin-conjugated PAMAM dendrimers is determined in a subsequent section. In the consecutive section, entropy measures are briefly described, and the analytical expression of the associated entropy measures of the TIs is derived. The predicted characteristics of the molecular structure under investigation are compared quantitatively and are presented graphically.

2.1. Topological Indices. " Topological Indices is the final result of a logic and mathematical procedure which transforms chemical information encoded within a symbolic representation of a molecule into a useful number or the result of some standardized experiment"—Todeschini & Consonni.[54]

TIs are obtained from fundamental information based on the molecular connection. They are basic numerical descriptors that provide a numerical value for the relationship between atom arrangement and intrinsic physical attributes of any chemical structure.[54] This predicts and supplies the data sets to QSAR/QSPR/QSTR (QSTR = quantitative structure−toxicity relationship) about the physiochemical and biochemical behavior of substances in terms of ecological impacts and medicinal aspects. The workflow is depicted in Figure 5.

The atoms of molecules are represented by dots, while the covalent bonds are represented by connecting lines. In chemical graphs, the dots are called vertices and the lines are called edges. Basic terminologies of the chemical graph corresponding to a molecular structure are provided in the Supporting Information.

The TIs are determined by applying some analytical techniques from graph theory, such as edge partition, vertex partition, eccentricity-based, and degree-based strategies. Many types of dendrimers, coronoid systems, benzoid systems, graphene, hexabenzocoronene, superphenalene, PAHs, carbon nanocones, antitubercular drugs, and drugs used for vitiligo treatment, are studied using degree-based indices.[36,55−75] Discrete adriatic indices, a category of degree-based indices, are used to analyze the conjugated structure.

Throughout this article, Ω denotes any chemical graph, $E(\Omega)$ signifies the collection of all edges $\{\partial,\partial_1,\partial_2,\partial_3...\}$, and $V(\Omega)$ is the set of all vertices $\{\alpha,\alpha_1,\alpha_2...\}$. Two vertices, α, and α_1, are neighboring if there exists an edge to link them. Let $\partial = \alpha\alpha_1$ represent an edge in the graph $E(G)$ with ends at α and α_1. The number of edges incident on any vertex α is the degree of vertex and is denoted by d_α. The total number of vertices in the graph is its order and is represented by $|V|$. The number of edges in graph Ω is its size and is represented by $|E|$.

The TIs considered for the study are all degree-based indices which are based on the edge-partition technique. The summation runs over all of the edge partitions in the respective molecular structure of the chemical compound. The number of edges present in each partition is called edge cardinality[48] and is denoted by $|E_i|$.

2.2. Discrete Adriatic Indices. This study evaluates and discusses a group of 16 bond additive descriptor indices based on the physiochemical properties they describe. The definition, terminology, nomenclature, and classification are provided in the Supporting Information. The index formulation, with their abbreviation, is given in the following.

1. Randic type lodeg index (good interpreter of heat capacity) is defined as

$$\mathrm{RLI}(\Omega) = \sum_{\partial\in E(\Omega)} \ln(d_\alpha)\ln(d_{\alpha_1})$$

2. Sum lordeg index (good interpreter of Log P value) is defined as

$$\mathrm{SLI}(\Omega) = \sum_{\partial\in E(\Omega)} [\sqrt{\ln(d_\alpha)} + \sqrt{\ln(d_{\alpha_1})}]$$

3. Inverse sum lordeg index (good interpreter of TSA) is defined as

$$\mathrm{ISLI}(\Omega) = \sum_{\partial\in E(\Omega)} \left(\frac{d_\alpha d_{\alpha_1}}{d_\alpha + d_{\alpha_1}}\right)$$

https://doi.org/10.1021/acsomega.4c00686
ACS Omega 2024, 9, 14558−14579

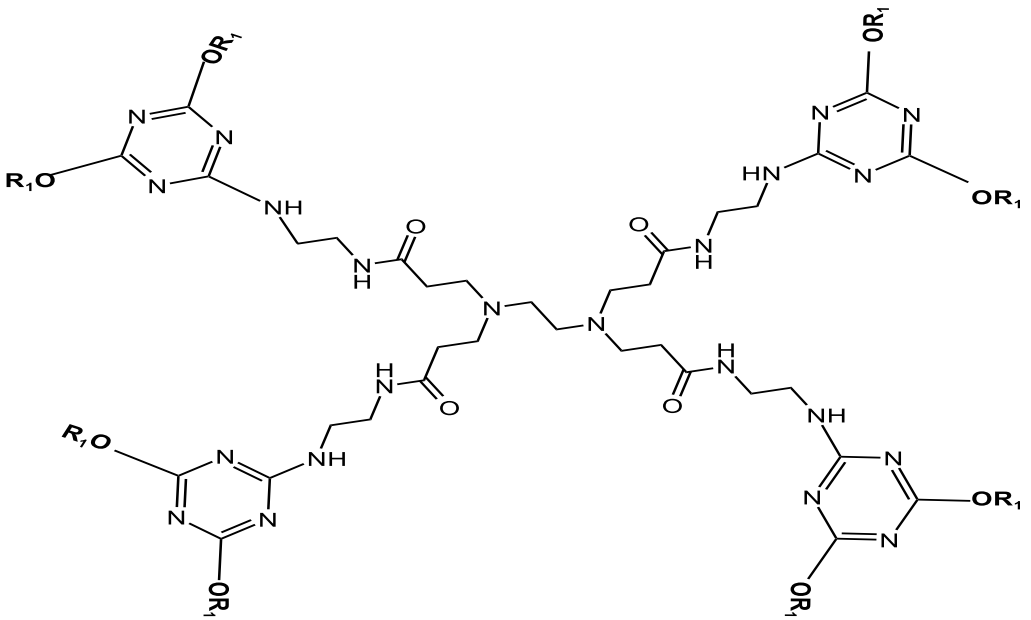

Figure 6. PAMAM dendrimer first generation bonded with R_1 represented as $\Omega_0(1)$.

4. Misbalance lodeg index (good interpreter of enthalpy of vaporization) is defined as

$$\mathrm{MLI}(\Omega) = \sum_{\partial \in E(\Omega)} |\ln(d_\alpha) - \ln(d_{\alpha_1})|$$

5. Misbalance losdeg index (good interpreter of enthalpy of vaporization) is defined as

$$\mathrm{MLSI}(\Omega) = \sum_{\partial \in E(\Omega)} |\ln^2(d_\alpha) - \ln^2(d_{\alpha_1})|$$

6. Misbalance indeg index (good interpreter of biological activity) is defined as

$$\mathrm{MII}(\Omega) = \sum_{\partial \in E(\Omega)} \left| \frac{1}{d_\alpha} - \frac{1}{d_{\alpha_1}} \right|$$

7. Misbalance irdeg index (good interpreter of enthalpy of vaporization) is defined as

$$\mathrm{MIRI}(\Omega) = \sum_{\partial \in E(\Omega)} \left| \frac{1}{\sqrt{d_\alpha}} - \frac{1}{\sqrt{d_{\alpha_1}}} \right|$$

8. Misbalance rodeg index (good interpreter of standard enthalpy of vaporization) is defined as

$$\mathrm{MRI}(\Omega) = \sum_{\partial \in E(\Omega)} |\sqrt{d_\alpha} - \sqrt{d_{\alpha_1}}|$$

9. Misbalance deg index (good interpreter of standard enthalpy of vaporization) is defined as

$$\mathrm{MDI}(\Omega) = \sum_{\partial \in E(\Omega)} |d_\alpha - d_{\alpha_1}|$$

10. Misbalance hadeg index (good interpreter of standard enthalpy of vaporization) is defined as

$$\mathrm{MHI}(\Omega) = \sum_{\partial \in E(\Omega)} \left| \left(\frac{1}{2}\right)^{d_\alpha} - \left(\frac{1}{2}\right)^{d_{\alpha_1}} \right|$$

11. Min-max rodeg index (good interpreter of enthalpy) is defined as

$$\mathrm{MMRI}(\Omega) = \sum_{\partial \in E(\Omega)} \sqrt{\frac{\min\{d_\alpha, d_{\alpha_1}\}}{\max\{d_\alpha, d_{\alpha_1}\}}}$$

12. Max-min rodeg index (good interpreter of density) is defined as

$$\mathrm{MMRDI}(\Omega) = \sum_{\partial \in E(\Omega)} \sqrt{\frac{\max\{d_\alpha, d_{\alpha_1}\}}{\min\{d_\alpha, d_{\alpha_1}\}}}$$

13. Max-min deg index (good interpreter of relative retention time) defined as

$$\mathrm{MMDI}(\Omega) = \sum_{\partial \in E(\Omega)} \frac{\max\{d_\alpha, d_{\alpha_1}\}}{\min\{d_\alpha, d_{\alpha_1}\}}$$

14. Max-min sdeg index (good interpreter of relative retention time) is defined as

$$\mathrm{MMSDI}(\Omega) = \sum_{\partial \in E(\Omega)} \left(\frac{\max\{d_\alpha, d_{\alpha_1}\}}{\min\{d_\alpha, d_{\alpha_1}\}} \right)^2$$

15. Symmetric division deg index (good interpreter of TSA) is defined as

$$\mathrm{SDDI}(\Omega) = \sum_{\partial \in E(\Omega)} \left(\frac{\min\{d_\alpha, d_{\alpha_1}\}}{\max\{d_\alpha, d_{\alpha_1}\}} + \frac{\max\{d_\alpha, d_{\alpha_1}\}}{\min\{d_\alpha, d_{\alpha_1}\}} \right)$$

16. Inverse sum indeg index (good interpreter of heat capacity) is defined as

$$\mathrm{ISI}(\Omega) = \sum_{\partial \in E(\Omega)} \frac{1}{\sqrt{\ln(d_\alpha)} + \sqrt{\ln(d_{\alpha_1})}}$$

An overview of the correlating physiochemical property is also mentioned along with the formulations presented above.[50]

2.3. Entropy Measures. Entropy is used in the study of complexity of molecular structures and their quantum chemical

https://doi.org/10.1021/acsomega.4c00686
ACS Omega 2024, 9, 14558−14579

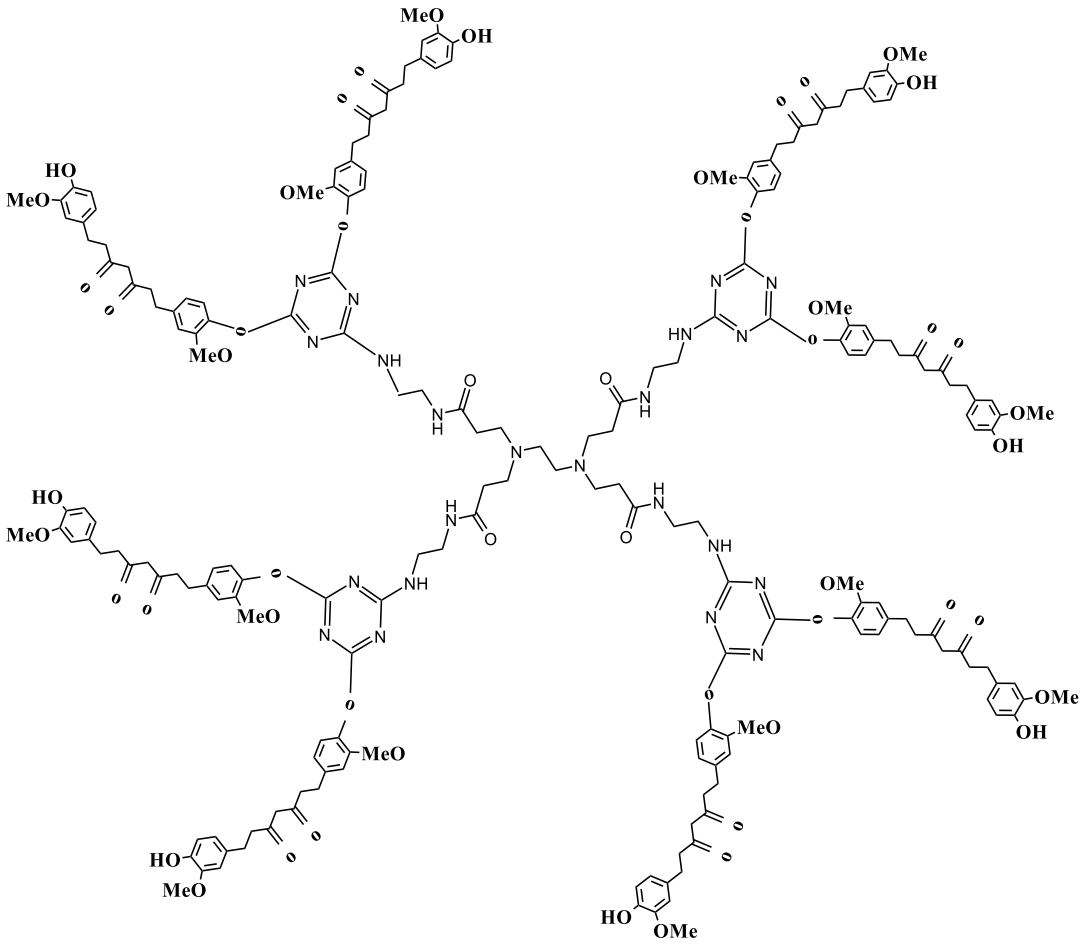

Figure 7. First-generation PAMAM dendrimer bonded with R_1, represented as $\Omega_1(2)$.

electron densities.[76] Dehmer developed graph entropies to quantify the topological information on chemical networks and graphs.[77] Estrada et al. examined the walk-based graph entropies and presented physically valid graph entropy indices.[78]

Information entropy is directly related to the formal carbon atom oxidation states and rotational symmetry numbers in several kinds of natural compounds.[56] Quantitatively characterizing a molecule structure and examining the chemical and biological characteristics of molecular graphs are two uses for entropy measures.[64]

The entropy measure for TI is defined by

$$\mathrm{ENT}_{\mathrm{TI}}(\Omega) = -\sum_{\partial \in E(G)} p_{\partial}\log(p_{\partial})$$

where the function p_{∂} is given by

$$p_e = \frac{f(\partial)}{\sum_{\partial \in E(\Omega)} f(\partial)} = \frac{f(\partial)}{\mathrm{TI}(\Omega)}$$

Therefore

$$\begin{aligned}\mathrm{ENT}_{\mathrm{TI}}(\Omega) &= -\sum_{\partial \in E(G)} p_{\partial}\log(p_{\partial}) \\ &= -\sum_{\partial \in E(G)} \frac{f(\partial)}{\mathrm{TI}(\Omega)}\log\left[\frac{f(\partial)}{\mathrm{TI}(\Omega)}\right] \\ &= -\frac{1}{\mathrm{TI}(\Omega)}\sum_{\partial \in E(G)} f(\partial)[\log f(\partial) - \log X(\Omega)]\end{aligned}$$

$$\mathrm{ENT}_{\mathrm{TI}}(\Omega) = \log[\mathrm{TI}(\Omega)] - \frac{1}{\mathrm{TI}(\Omega)}\sum_{\partial \in E(G)} f(\partial)\log f(\partial)$$

In literature, prominent illustrations of degree-based entropy metrics being applied to comprehend chemical structures.[79]

3. CURCUMIN—PAMAM DENDRIMERS (CD)

The peripheral primary amino groups of PAMAM dendrimers of various generations have been modified with curcumin (residue R_1). The synthesized modified PAMAM dendrimers of zero generation (core) at the first growth stage are illustrated in Figure 6.

$\Omega_{\gamma}[\mu]$ represents the graph of the molecular structure, γ represents the generation, and μ represents the growth stage of the corresponding generation. The first and second generations with covalently bonded curcumin residues were considered for the study.[44]

3.1. First Generation (CD_1). $\Omega_1[2]$ represents the first-generation curcumin-conjugated PAMAM dendrimer in the

https://doi.org/10.1021/acsomega.4c00686
ACS Omega 2024, 9, 14558−14579

second development stage. The properties of $\Omega_1[2]$ (denoted CD_1) are examined. The size of CD_1 is $2^{\mu+1}(71) + 3$ and the order of CD_1 is $2^{\mu+1}(68) + 4$. The vertex set is partitioned into three categories as $2^{\mu+1}(11) + 4$, $2^{\mu+1}(35) + 6$, and $2^{\mu+1}(21) + 2$, which are the cardinality of vertices of one, two, and three degrees, respectively. The chemical structure of $\Omega_1[2]$ is illustrated in Figure 7.

By edge partition, $E(\Omega)$ of CD_1 is divided into four parts as follows

$$\begin{aligned} E_1(CD_1) &= E_{13} \\ &= \{\alpha\alpha_1 \in E(CD_1): d_\alpha(CD_1) \\ &= 1 \text{ and } E(CD_1) \\ &= 3\} \end{aligned}$$

$$\begin{aligned} E_2(CD_1) &= E_{23} \\ &= \{\alpha\alpha_1 \in E(CD_1): d_\alpha(CD_1) \\ &= 2 \text{ and } E(CD_1) \\ &= 2\} \end{aligned}$$

$$\begin{aligned} E_3(CD_1) &= E_{23} \\ &= \{\alpha\alpha_1 \in E(CD_1): d_\alpha(CD_1) \\ &= 2 \text{ and } E(CD_1) \\ &= 3\} \end{aligned}$$

$$\begin{aligned} E_4(CD_1) &= E_{33} \\ &= \{\alpha\alpha_1 \in E(CD_1): \ d_\alpha(CD_1) \\ &= 3 \text{ and } E(CD_1) \\ &= 3\} \end{aligned}$$

The cardinality of every partition of $\mathbf{CD}_1$ represented by $|E_i|$ is stated in Table 4.

Table 4. Edge Partition and Cardinality of $\Omega_1(2)$

E_i	(d_α, d_{α_1})	$\lvert E_i\rvert$
E_1	(1,2)	$(2^{\mu+1})8 + 4$
E_2	(2,2)	$(2^{\mu+1})14 + 7$
E_3	(2,3)	$(2^{\mu+1})44 + 2$
E_4	(3,3)	$(2^{\mu+1})4$

Theorem 1: For the molecular structures of the first-generation curcumin-conjugated PAMAM dendrimer represented in Figure $\mathbf{CD}_1$, $\mu \geq 1$, with edge partitions as $|E_1| = (2^{\mu+1})8 + 4$, $|E_2| = (2^{\mu+1})14 + 7$, $|E_3| = (2^{\mu+1})44 + 2$, and $|E_4| = (2^{\mu+1})4$, the adriatic indices are

$$1\ \mathrm{RLI}[(CD_1)(\mu)] = (45.0601)2^{\mu+1} + 4.8862$$

$$2\ \mathrm{SLI}[(CD_1)(\mu)] = (122.8168)2^{\mu+1} + 19.6084$$

$$3\ \mathrm{ISLI}[(CD_1)(\mu)] = (78.8)2^{\mu+1} + 12.4$$

$$4\ \mathrm{MLI}[(CD_1)(\mu)] = (26.6264)2^{\mu+1} + 5.2052$$

$$5\ \mathrm{MLSI}[(CD_1)(\mu)] = (12.7408)2^{\mu+1} + 0.92112$$

$$6\ \mathrm{MII}[(CD_1)(\mu)] = (12.6667)2^{\mu+1} + 3.0000$$

$$7\ \mathrm{MIRI}[(CD_1)(\mu)] = (9.0832)2^{\mu+1} + 1.9466$$

$$8\ \mathrm{MRI}[(CD_1)(\mu)] = (19.848)2^{\mu+1} + 3.564$$

$$9\ \mathrm{MDI}[(CD_1)(\mu)] = (60)2^{\mu+1} + 10$$

$$10\ \mathrm{MHI}[(CD_1)(\mu)] = (8.5)2^{\mu+1} + 1.75$$

$$11\ \mathrm{MMRI}[(CD_1)(\mu)] = (58.5446)2^{\mu+1} + 10.9423$$

$$12\ \mathrm{MMRDI}[(CD_1)(\mu)] = (85.7445)2^{\mu+1} + 16.3776$$

$$13\ \mathrm{MMDI}[(CD_1)(\mu)] = (108)2^{\mu+1} + 22$$

$$14\ \mathrm{MMSDI}[(CD_1)(\mu)] = (189)2^{\mu+1} + 47.5$$

$$15\ \mathrm{SDDI}[(CD_1)(\mu)] = (67.0667)2^{\mu+1} + 31.663$$

$$16\ \mathrm{ISI}[(CD_1)(\mu)] = (37.6266)2^{\mu+1} + 9.0844$$

Following is the proof

$$\begin{aligned} 1\ \mathrm{RLI}[(CD_1)(\mu)] &= \sum_{uv \in E(G)} \ln(d_\alpha)\ln(d_{\alpha_1}) \\ &= [(\ln(1)\ln(3)(82^{\mu+1} + 4)) \\ &\quad + (\ln(2)\ln(2))(14.22^{\mu+1} + 7) \\ &\quad + (\ln(2)\ln(3))(442^{\mu+1} + 2) \\ &\quad + (\ln(3)\ln(3))(42^{\mu+1})] \\ &= (45.0601)2^{\mu+1} + 4.8862 \end{aligned}$$

The proof of other TIs is analogous to that of RLI.

Theorem 2: For the molecular structure of PAMAM dendrimer of first generation with curcumin conjugation (CD_1), $\mu \geq 1$, the entropy measures of adriatic indices are

$$\begin{aligned} &1\ \mathrm{ENT}_{\mathrm{RLI}}(CD_1)(\mu) \\ &= \log[(45.0601)2^{\mu+1} + 4.8862] \\ &\quad + \frac{[(7.597)2^{\mu+1} + 0.9366]}{[(45.0601)2^{\mu+1} + 4.8862]} \end{aligned}$$

$$\begin{aligned} &2\ \mathrm{ENT}_{\mathrm{SLI}}(CD_1)(\mu) \\ &= \log[(122.8168)2^{\mu+1} + 19.6084] \\ &\quad + \frac{[(28.6799)2^{\mu+1} + 3.34786]}{[(122.8168)2^{\mu+1} + 19.6084]} \end{aligned}$$

$$\begin{aligned} &3\ \mathrm{ENT}_{\mathrm{ISLI}}(CD_1)(\mu) \\ &= \log[(78.8)2^{\mu+1} + 12.4] - \frac{[(3.4311)2^{\mu+1} - 0.1847]}{[(78.8)2^{\mu+1} + 12.44]} \end{aligned}$$

$$\begin{aligned} &4\ \mathrm{ENT}_{\mathrm{MLI}}(CD_1)(\mu) \\ &= \log[(26.6264)2^{\mu+1} + 5.2052] \\ &\quad + \frac{[(6.6822)2^{\mu+1} + 0.15708]}{[(26.6264)2^{\mu+1} + 5.2052]} \end{aligned}$$

https://doi.org/10.1021/acsomega.4c00686
ACS Omega 2024, 9, 14558−14579

$$5\ \mathrm{ENT}_{\mathrm{MLSI}}(\mathrm{CD}_1)(\mu) = \log[(12.7408)2^{\mu+1} + 0.9211] + \frac{[(7.5422)2^{\mu+1} + 0.6939]}{[(53.2376)2^{\mu+1} + 10.4108]}$$

$$6\ \mathrm{ENT}_{\mathrm{MII}}(\mathrm{CD}_1)(\mu) = \log[(12.6667)2^{\mu+1} + 3] + \frac{[(6.6455)2^{\mu+1} + 0.9883]}{[(12.6667)2^{\mu+1} + 3]}$$

$$7\ \mathrm{ENT}_{\mathrm{MIRI}}(\mathrm{CD}_1)(\mu) = \log[(9.0832)2^{\mu+1} + 1.9466] + \frac{[(6.3244)2^{\mu+1} + 0.862]}{[(9.0832)2^{\mu+1} + 1.6466]}$$

$$8\ \mathrm{ENT}_{\mathrm{MRI}}(\mathrm{CD}_1)(\mu) = \log[(19.848)2^{\mu+1} + 3.564] + \frac{[(7.136)2^{\mu+1} + 0.687]}{[(19.848)2^{\mu+1} + 3.564]}$$

$$9\ \mathrm{ENT}_{\mathrm{MDI}}(\mathrm{CD}_1)(\mu) = \log[(60)2^{\mu+1} + 10] - \frac{[(4.816)2^{\mu+1} + 2.408]}{[(60)2^{\mu+1} + 10]}$$

$$10\ \mathrm{ENT}_{\mathrm{MHI}}(\mathrm{CD}_1)(\mu) = \log[(8.25)2^{\mu+1} + 1.75] + \frac{[(7.903)2^{\mu+1} + 0.9415]}{[(8.25)2^{\mu+1} + 1.75]}$$

$$11\ \mathrm{ENT}_{\mathrm{MMRI}}(\mathrm{CD}_1)(\mu) = \log[(58.5446)2^{\mu+1} + 10.9423] + \frac{[(4.2649)2^{\mu+1} + 0.6947]}{[(58.5446)2^{\mu+1} + 10.9423]}$$

$$12\ \mathrm{ENT}_{\mathrm{MMRDI}}(\mathrm{CD}_1)(\mu) = \log[(85.7445)2^{\mu+1} + 16.3776] - \frac{[(8.0466)2^{\mu+1} + 1.8675]}{[(87.7445)2^{\mu+1} + 16.377]}$$

$$13\ \mathrm{ENT}_{\mathrm{MMDI}}(\mathrm{CD}_1)(\mu) = \log[(108)2^{\mu+1} + 22] - \frac{[(23.063)2^{\mu+1} + 6.252]}{[(108)2^{\mu+1} + 22]}$$

$$14\ \mathrm{ENT}_{\mathrm{MMSDI}}(\mathrm{CD}_1)(\mu) = \log[(189)2^{\mu+1} + 47.5] - \frac{[(103.534)2^{\mu+1} + 35.929]}{[(189)2^{\mu+1} + 4.75]}$$

$$15\ \mathrm{ENT}_{\mathrm{SDDI}}(\mathrm{CD}_1)(\mu) = \log[(67.066)2^{\mu+1} + 31.663] - \frac{[(56.8)2^{\mu+1} + 15.04]}{[(67.066)2^{\mu+1} + 31.663]}$$

$$16\ \mathrm{ENT}_{\mathrm{ISI}}(\mathrm{CD}_1)(\mu) = \log[(37.6266)2^{\mu+1} + 9.0844] + \frac{[(25.94)2^{\mu+1} + 1.138]}{[(37.6266)2^{\mu+1} + 31.663]}$$

Following is the proof

$$1\ \mathrm{ENT}_{\mathrm{RLI}}(\mathrm{CD}_1)(\mu) = \log(\mathrm{RLI})(\mathrm{CD}_1)(\mu) - \frac{1}{\mathrm{RLI}(\mathrm{CD}_1)(\mu)} \sum f(\partial)\log f(\partial)$$

$$= \log(\mathrm{RLI})(\mathrm{CD}_1)(\mu) - \frac{1}{\mathrm{RLI}(\mathrm{CD}_1)(\mu)} \sum \ln(d_\alpha)\ln(d_{\alpha_1})\log[\ln(d_\alpha)\ln(d_{\alpha_1})]$$

$$= \log(\mathrm{RLI})(\mathrm{CD}_1)(\mu) - \frac{1}{\mathrm{RLI}(\mathrm{CD}_1)(\mu)} \{\ln(1)\ln(3)\log[\ln(1)\ln(3)](82^{n\mu+1} + 4) + \ln(2)\ln(2)\log[\ln(2)\ln(2)](142^{n\mu+1} + 7) + \ln(2)\ln(3)\log[\ln(2)\ln(3)](442^{n\mu+1} + 2) + \ln(3)\ln(3)\log[\ln(3)\ln(3)](42^{n\mu+1})\}$$

$$= \log[(45.0601)2^{\mu+1} + 4.8862] + \frac{[(7.597)2^{\mu+1} + 0.9366]}{[(45.0601)2^{\mu+1} + 4.8862]}$$

$$2\ \mathrm{ENT}_{\mathrm{SLI}}(\mathrm{CD}_1)(\mu) = \log(\mathrm{SLI})(\mathrm{CD}_1)(\mu) - \frac{1}{\mathrm{SLI}(\mathrm{CD}_1)(\mu)} \sum f(\partial)\log f(\partial)$$

$$= \log(\mathrm{SLI})(\mathrm{CD}_1)(\mu) - \frac{1}{\mathrm{SLI}(\mathrm{CD}_1)(\mu)} \sum \sqrt{\ln(d_u)} + \sqrt{\ln(d_v)}\log[\sqrt{\ln(d_u)} + \sqrt{\ln(d_v)}]$$

$$= \log(\mathrm{SLI})(\mathrm{CD}_1)(\mu) - \frac{1}{\mathrm{SLI}(\mathrm{CD}_1)(\mu)} \{[\sqrt{\ln(1)} + \sqrt{\ln(3)}]\log[\sqrt{\ln(1)} + \sqrt{\ln(3)}](82^{\mu+1} + 4) + [\sqrt{\ln(2)} + \sqrt{\ln(2)}]\log[\sqrt{\ln(2)} + \sqrt{\ln(2)}](142^{\mu+1} + 7) + [\sqrt{\ln(2)} + \sqrt{\ln(3)}]\log[\sqrt{\ln(2)} + \sqrt{\ln(3)}](442^{\mu+1} + 2) + [\sqrt{\ln(3)} + \sqrt{\ln(3)}]\log[\sqrt{\ln(3)} + \sqrt{\ln(3)}](42^{\mu+1})\}$$

$$= \log[(122.8168)2^{\mu+1} + 19.6084] + \frac{[(28.6799)2^{\mu+1} + 3.3478]}{[(122.8168)2^{\mu+1} + 19.6084]}$$

https://doi.org/10.1021/acsomega.4c00686
ACS Omega 2024, 9, 14558−14579

$$3\ \mathrm{ENT}_{\mathrm{ISLI}}(\mathrm{CD}_1)(\mu) = \log(\mathrm{ISLI})(\mathrm{CD}_1)(\mu) - \frac{1}{\mathrm{ISLI}(\mathrm{CD}_1)(n\mu)} \sum f(\partial)\log f(\partial)$$

$$= \log(\mathrm{ISLI})(\mathrm{CD}_1)(\mu) - \frac{1}{\mathrm{ISLI}(\mathrm{CD}_1)(\mu)} \sum \frac{d_u d_v}{d_u + d_v}\log\left(\frac{d_u d_v}{d_u + d_v}\right)$$

$$= \log(\mathrm{ISLI})(\mathrm{CD}_1)(\mu) - \frac{1}{\mathrm{ISLI}(\mathrm{CD}_1)(\mu)} \left\{\frac{1\times 3}{1+3}\log\left(\frac{1\times 3}{1+3}\right)(8.2^{\mu+1}+4) + \frac{2\times 2}{2+2}\log\left(\frac{2\times 2}{2+2}\right)(14.2^{\mu+1}+7) + \frac{2\times 3}{2+3}\log\left(\frac{2\times 3}{2+3}\right)(44.2^{\mu+1}+2) + \frac{3\times 3}{3+3}\log\left(\frac{3\times 3}{3+3}\right)(4.2^{\mu+1})\right\}$$

$$= \log[(78.8)2^{\mu+1} + 12.4] - \frac{[(3.4311)2^{\mu+1} - 0.184]}{[(78.8)2^{\mu+1} + 12.4]}$$

$$4\ \mathrm{ENT}_{\mathrm{MLI}}(\mathrm{CD}_1)(\mu) = \log(\mathrm{MLI})(\mathrm{CD}_1)(\mu) - \frac{1}{\mathrm{MLI}(\mathrm{CD}_1)(\mu)} \sum f(\partial)\log f(\partial)$$

$$= \log(\mathrm{MLI})(\mathrm{CD}_1)(\mu) - \frac{1}{\mathrm{MLI}(\mathrm{CD}_1)(\mu)} \{|\ln(1) - \ln(3)|\log|\ln(1) - \ln(3)|| (8.2^{\mu+1}+4) + |\ln(2) - \ln(2)| \log|\ln(1) - \ln(3)|(14.2^{\mu+1}+7) + |\ln(2) - \ln(3)|\log|\ln(1) - \ln(3)|| (44.2^{\mu+1}+2) + |\ln(3) - \ln(3)| \log|\ln(1) - \ln(3)|(4.2^{\mu+1})\}$$

$$= \log[(26.6264)2^{\mu+1} + 5.2052] + \frac{[(6.6822)2^{\mu+1} + 0.15708]}{[(26.6264)2^{\mu+1} + 5.2052]}$$

$$5\ \mathrm{ENT}_{\mathrm{MLSI}}(\mathrm{CD}_1)(\mu) = \log(\mathrm{MLSI})(\mathrm{CD}_1)(\mu) - \frac{1}{\mathrm{MLSI}(\mathrm{CD}_1)(\mu)} \sum f(\partial)\log f(\partial)$$

$$= \log(MLSI)(CD_1)(\mu) - \frac{1}{MLSI(CD_1)(\mu)} \{|\ln^2(1) - \ln^2(3)| \log|\ln^2(1) - \ln^2(3)|(82^{\mu+1}+7) + |\ln^2(2) - \ln^2(2)| \log|\ln^2(2) - \ln^2(2)|(142^{\mu+1}+7) + |\ln^2(2) - \ln^2(3)| \log|\ln^2(2) - \ln^2(3)|(442^{\mu+1}+2) + |\ln^2(3) - \ln^2(3)| \log|\ln^2(3) - \ln^2(3)|(42^{\mu+1})\}$$

$$= \log[(12.7408)2^{\mu+1} + 0.9211] + \frac{[(7.5422)2^{\mu+1} + 0.6939]}{[(12.7408)2^{\mu+1} + 0.9211]}$$

$$6\ \mathrm{ENT}_{\mathrm{MII}}(\mathrm{CD}_1)(\mu) = \log(\mathrm{MII})(\mathrm{CD}_1)(\mu) - \frac{1}{\mathrm{MII}(\mathrm{CD}_1)(\mu)} \sum f(\partial)\log f(\partial)$$

$$= \log(\mathrm{MII})(\mathrm{CD}_1)(\mu) - \frac{1}{\mathrm{MII}(\mathrm{CD}_1)(\mu)} \left\{\left|\frac{1}{1}-\frac{1}{3}\right| \log\left|\frac{1}{1}-\frac{1}{3}\right|(82^{\mu+1}+4) + \left|\frac{1}{2}-\frac{1}{2}\right|\log\left|\frac{1}{2}-\frac{1}{2}\right| (142^{\mu+1}+7) + \left|\frac{1}{2}-\frac{1}{3}\right| \log\left|\frac{1}{2}-\frac{1}{3}\right|(442^{\mu+1}+2) + \left|\frac{1}{3}-\frac{1}{3}\right|\log\left|\frac{1}{3}-\frac{1}{3}\right|(42^{\mu+1})\right\}$$

$$= \log[(12.6667)2^{\mu+1} + 3] + \frac{[(6.6455)2^{\mu+1} + 0.9883]}{[(12.6667)2^{\mu+1} + 3]}$$

https://doi.org/10.1021/acsomega.4c00686
ACS Omega 2024, 9, 14558−14579

$$7\ \mathrm{ENT}_{\mathrm{MIRI}}(\mathrm{CD}_1)(\mu) = \log(\mathrm{MIRI})(\mathrm{CD}_1)(\mu) - \frac{1}{\mathrm{MIRI}(\mathrm{CD}_1)(\mu)} \sum f(\partial)\log f(\partial)$$

$$= \log(\mathrm{MIRI})(\mathrm{CD}_1)(\mu) - \frac{1}{\mathrm{MIRI}(\mathrm{CD}_1)(\mu)} \left\{ \left|\frac{1}{\sqrt{1}} - \frac{1}{\sqrt{3}}\right| \log\left|\frac{1}{\sqrt{1}} - \frac{1}{\sqrt{3}}\right| (82^{\mu+1} + 4) + \left|\frac{1}{\sqrt{2}} - \frac{1}{\sqrt{2}}\right| \log\left|\frac{1}{\sqrt{2}} - \frac{1}{\sqrt{2}}\right| (142^{\mu+1} + 7) + \left|\frac{1}{\sqrt{2}} - \frac{1}{\sqrt{3}}\right| \log\left|\frac{1}{\sqrt{2}} - \frac{1}{\sqrt{3}}\right| (442^{\mu+1} + 2) + \left|\frac{1}{\sqrt{3}} - \frac{1}{\sqrt{3}}\right| \log\left|\frac{1}{\sqrt{3}} - \frac{1}{\sqrt{3}}\right| (42^{\mu+1}) \right\}$$

$$= \log[(9.0832)2^{\mu+1} + 1.9466] + \frac{[(6.3244)2^{\mu+1} + 0.862]}{[(9.0832)2^{\mu+1} + 1.6466]}$$

$$8\ \mathrm{ENT}_{\mathrm{MRII}}(\mathrm{CD}_1)(\mu) = \log(\mathrm{MRII})(\mathrm{CD}_1)(\mu) - \frac{1}{\mathrm{MRII}(\mathrm{CD}_1)(\mu)} \sum f(\partial)\log f(\partial)$$

$$= \log(\mathrm{MRII})(\mathrm{CD}_1)(\mu) - \frac{1}{\mathrm{MRII}(\mathrm{CD}_1)(\mu)} \left\{ \left|\frac{1}{\sqrt{1}} - \frac{1}{\sqrt{3}}\right| \log\left|\frac{1}{\sqrt{1}} - \frac{1}{\sqrt{3}}\right| (82^{\mu+1} + 4) + \left|\frac{1}{\sqrt{2}} - \frac{1}{\sqrt{2}}\right| \log\left|\frac{1}{\sqrt{2}} - \frac{1}{\sqrt{2}}\right| (142^{\mu+1} + 7) + \left|\frac{1}{\sqrt{2}} - \frac{1}{\sqrt{3}}\right| \log\left|\frac{1}{\sqrt{2}} - \frac{1}{\sqrt{3}}\right| (442^{\mu+1} + 2) + \left|\frac{1}{\sqrt{3}} - \frac{1}{\sqrt{3}}\right| \log\left|\frac{1}{\sqrt{3}} - \frac{1}{\sqrt{3}}\right| (42^{\mu+1}) \right\}$$

$$= \log[(19.848)2^{\mu+1} + 3.564] + \frac{[(7.136)2^{\mu+1} + 0.687]}{[(19.848)2^{\mu+1} + 3.564]}$$

$$9\ \mathrm{ENT}_{\mathrm{MDI}}(\mathrm{CD}_1)(\mu) = \log(\mathrm{MDI})(\mathrm{CD}_1)(\mu) - \frac{1}{\mathrm{MDI}(\mathrm{CD}_1)(\mu)} \sum f(\partial)\log f(\partial)$$

$$= \log(\mathrm{MDI})(\mathrm{CD}_1)(\mu) - \frac{1}{\mathrm{MDI}(\mathrm{CD}_1)(\mu)} \{|1 - 3|\log|1 - 3|(82^{\mu+1} + 4) + |2 - 2|\log|2 - 2|(142^{\mu+1} + 7) + |2 - 3|\log|2 - 3|(442^{\mu+1} + 2) + |3 - 3|\log|3 - 3|(42^{\mu+1})\}$$

$$= \log[(60)2^{\mu+1} + 10] - \frac{[(4.816)2^{\mu+1} + 2.408]}{[(60)2^{\mu+1} + 10]}$$

$$10\ \mathrm{ENT}_{\mathrm{MHI}}(\mathrm{CD}_1)(\mu) = \log(\mathrm{MHI})(\mathrm{CD}_1)(\mu) - \frac{1}{\mathrm{MHI}(\mathrm{CD}_1)(\mu)} \sum f(\partial)\log f(\partial)$$

$$= \log(\mathrm{MHI})(\mathrm{CD}_1)(\mu) - \frac{1}{\mathrm{MHI}(\mathrm{CD}_1)(\mu)} \left\{ \left|\left(\frac{1}{2}\right)^1 - \left(\frac{1}{2}\right)^3\right| \log\left|\left(\frac{1}{2}\right)^1 - \left(\frac{1}{2}\right)^3\right| (82^{n\mu+1} + 4) + \left|\left(\frac{1}{2}\right)^2 - \left(\frac{1}{2}\right)^2\right| \log\left|\left(\frac{1}{2}\right)^2 - \left(\frac{1}{2}\right)^2\right| (142^{\mu+1} + 7) + \left|\left(\frac{1}{2}\right)^2 - \left(\frac{1}{2}\right)^3\right| \log\left|\left(\frac{1}{2}\right)^2 - \left(\frac{1}{2}\right)^3\right| (442^{\mu+1} + 2) + \left|\left(\frac{1}{2}\right)^3 - \left(\frac{1}{2}\right)^3\right| \log\left|\left(\frac{1}{2}\right)^3 - \left(\frac{1}{2}\right)^3\right| (42^{\mu+1}) \right\}$$

$$= \log[(8.25)2^{\mu+1} + 1.75] + \frac{[(7.903)2^{\mu+1} + 0.9415]}{[(8.25)2^{\mu+1} + 1.75]}$$

https://doi.org/10.1021/acsomega.4c00686
ACS Omega 2024, 9, 14558−14579

$$11\ \mathrm{ENT}_{\mathrm{MMRI}}(\mathrm{CD}_1)(\mu) = \log(\mathrm{MMRI})(\mathrm{CD}_1)(\mu) - \frac{1}{\mathrm{MMRI}(\mathrm{CD}_1)(\mu)} \sum f(\partial)\log f(\partial)$$

$$= \log(\mathrm{MMRI})(\mathrm{CD}_1)(\mu) - \frac{1}{\mathrm{MMRI}(\mathrm{CD}_1)(\mu)} \left\{ \sqrt{\frac{\min\{1,3\}}{\max\{1,3\}}} \log\left[\sqrt{\frac{\min\{1,3\}}{\max\{1,3\}}} \right] (82^{\mu+1}+4) + \sqrt{\frac{\min\{2,2\}}{\max\{2,2\}}} \log\left[\sqrt{\frac{\min\{2,2\}}{\max\{2,2\}}} \right] (142^{\mu+1}+7) + \sqrt{\frac{\min\{2,3\}}{\max\{2,3\}}} \log\left[\sqrt{\frac{\min\{2,3\}}{\max\{2,3\}}} \right] (442^{\mu+1}+2) + \sqrt{\frac{\min\{3,3\}}{\max\{3,3\}}} \log\left[\sqrt{\frac{\min\{3,3\}}{\max\{3,3\}}} \right] (42^{\mu+1}) \right\}$$

$$= \log[(58.5446)2^{\mu+1} + 10.9423] + \frac{[(4.2649)2^{\mu+1} + 0.6947]}{[(58.5446)2^{\mu+1} + 10.9423]}$$

$$12\ \mathrm{ENT}_{\mathrm{MMRDI}}(\mathrm{CD}_1)(\mu) = \log(\mathrm{MMRDI})(\mathrm{CD}_1)(\mu) - \frac{1}{\mathrm{MMRDI}(\mathrm{CD}_1)(\mu)} \sum f(\partial)\log f(\partial)$$

$$= \log(\mathrm{MMRDI})(\mathrm{CD}_1)(\mu) - \frac{1}{\mathrm{MMRDI}(\mathrm{CD}_1)(\mu)} \left\{ \sqrt{\frac{\max\{1,3\}}{\min\{1,3\}}} \log\left[\sqrt{\frac{\max\{1,3\}}{\min\{1,3\}}} \right] (82^{\mu+1}+4) + \sqrt{\frac{\max\{2,2\}}{\min\{2,2\}}} \log\left[\sqrt{\frac{\max\{2,2\}}{\min\{2,2\}}} \right] (142^{\mu+1}+7) + \sqrt{\frac{\max\{2,3\}}{\min\{2,3\}}} \log\left[\sqrt{\frac{\max\{2,3\}}{\min\{2,3\}}} \right] (442^{\mu+1}+2) + \sqrt{\frac{\max\{3,3\}}{\min\{3,3\}}} \log\left[\sqrt{\frac{\max\{3,3\}}{\min\{3,3\}}} \right] (42^{\mu+1}) \right\}$$

$$= \log[(85.744)2^{\mu+1} + 16.3774] - \frac{[(8.0466)2^{\mu+1} + 1.8675]}{[(87.744)2^{\mu+1} + 16.3774]}$$

https://doi.org/10.1021/acsomega.4c00686
ACS Omega 2024, 9, 14558−14579

$$13\ \mathrm{ENT}_{\mathrm{MMDI}}(\mathrm{CD}_1)(\mu) = \log(\mathrm{MMDI})(\mathrm{CD}_1)(\mu) - \frac{1}{\mathrm{MMDI}(\mathrm{CD}_1)(\mu)} \sum f(\partial)\log f(\partial)$$

$$= \log(\mathrm{MMDI})(\mathrm{CD}_1)(\mu) - \frac{1}{\mathrm{MMDI}(\mathrm{CD}_1)(\mu)} \left\{ \frac{\max\{1,3\}}{\min\{1,3\}} \log\left[\frac{\max\{1,3\}}{\min\{1,3\}}\right] (82^{\mu+1}+4) + \frac{\max\{2,2\}}{\min\{2,2\}} \log\left[\frac{\max\{2,2\}}{\min\{2,2\}}\right] (142^{\mu+1}+7) + \frac{\max\{2,3\}}{\min\{2,3\}} \log\left[\frac{\max\{2,3\}}{\min\{2,3\}}\right] (442^{\mu+1}+2) + \frac{\max\{3,3\}}{\min\{3,3\}} \log\left[\frac{\max\{3,3\}}{\min\{3,3\}}\right] (42^{\mu+1}) \right\}$$

$$= \log[(108)2^{\mu+1}+22] - \frac{[(23.063)2^{\mu+1}+6.252]}{[(108)2^{\mu+1}+22]}$$

$$14\ \mathrm{ENT}_{\mathrm{MMSDI}}(\mathrm{CD}_1)(\mu) = \log(\mathrm{MMSDI})(\mathrm{CD}_1)(\mu) - \frac{1}{\mathrm{MMSDI}(\mathrm{CD}_1)(\mu)} \sum f(\partial)\log f(\partial)$$

$$= \log(\mathrm{MMSDI})(\mathrm{CD}_1)(\mu) - \frac{1}{\mathrm{MMSDI}(\mathrm{CD}_1)(\mu)} \left\{ \left(\frac{\max\{1,3\}}{\min\{1,3\}}\right)^2 \log\left[\left(\frac{\max\{1,3\}}{\min\{1,3\}}\right)^2 \right] (82^{\mu+1}+4) + \left(\frac{\max\{2,2\}}{\min\{2,2\}}\right)^2 \log\left[\left(\frac{\max\{2,2\}}{\min\{2,2\}}\right)^2 \right] (142^{\mu+1}+7) + \left(\frac{\max\{2,3\}}{\min\{2,3\}}\right)^2 \log\left[\left(\frac{\max\{2,3\}}{\min\{2,3\}}\right)^2 \right] (442^{\mu+1}+2) + \left(\frac{\max\{3,3\}}{\min\{3,3\}}\right)^2 \log\left[\left(\frac{\max\{3,3\}}{\min\{3,3\}}\right)^2 \right] (42^{\mu+1}) \right\}$$

$$= \log[(189)2^{\mu+1}+47.5] - \frac{[(103.534)2^{\mu+1}+35.929]}{[(189)2^{\mu+1}+4.75]}$$

https://doi.org/10.1021/acsomega.4c00686
ACS Omega 2024, 9, 14558−14579

$$15\ \mathrm{ENT}_{\mathrm{SDDI}}(\mathrm{CD}_1)(\mu) = \log(\mathrm{SDDI})(\mathrm{CD}_1)(\mu) - \frac{1}{\mathrm{SDDI}(\mathrm{CD}_1)(\mu)} \sum f(\partial)\log f(\partial)$$

$$= \log(\mathrm{SDDI})(\mathrm{CD}_1)(\mu) - \frac{1}{\mathrm{SDDI}(\mathrm{CD}_1)(\mu)} \left\{ \left(\frac{\min\{1,3\}}{\max\{1,3\}} + \frac{\max\{1,3\}}{\min\{1,3\}} \right) \log\left[\left(\frac{\min\{1,3\}}{\max\{1,3\}} + \frac{\max\{1,3\}}{\min\{1,3\}} \right) \right] (82^{\mu+1} + 4) + \left(\frac{\min\{2,2\}}{\max\{2,2\}} + \frac{\max\{2,2\}}{\min\{2,2\}} \right) \log\left[\left(\frac{\min\{2,2\}}{\max\{2,2\}} + \frac{\max\{2,2\}}{\min\{2,2\}} \right) \right] (142^{\mu+1} + 7) + \left(\frac{\min\{2,3\}}{\max\{2,3\}} + \frac{\max\{2,3\}}{\min\{2,3\}} \right) \log\left[\left(\frac{\min\{2,3\}}{\max\{2,3\}} + \frac{\max\{2,3\}}{\min\{2,3\}} \right) \right] (442^{\mu+1} + 2) + \left(\frac{\min\{3,3\}}{\max\{3,3\}} + \frac{\max\{3,3\}}{\min\{3,3\}} \right) \log\left[\left(\frac{\min\{3,3\}}{\max\{3,3\}} + \frac{\max\{3,3\}}{\min\{3,3\}} \right) \right] (42^{\mu+1}) \right\}$$

$$= \log[(67.066)2^{\mu+1} + 31.663] - \frac{[(56.8)2^{\mu+1} + 15.04]}{[(67.066)2^{\mu+1} + 31.663]}$$

$$16\mathrm{ENT}_{\mathrm{ISI}}(\mathrm{CD}_1)(\mu) = \log(\mathrm{ISI})(\mathrm{CD}_1)(\mu) - \frac{1}{\mathrm{ISI}(\mathrm{CD}_1)(\mu)} \sum f(\partial)\log f(\partial)$$

$$= \log(\mathrm{ISI})(\mathrm{CD}_1)(\mu) - \frac{1}{\mathrm{ISI}(\mathrm{CD}_1)(\mu)} \left\{ \frac{1}{(\sqrt{\ln(1)} + \sqrt{\ln(3)})} \log\left[\frac{1}{(\sqrt{\ln(1)} + \sqrt{\ln(3)})} \right] (82^{\mu+1} + 4) + \frac{1}{(\sqrt{\ln(2)} + \sqrt{\ln(2)})} \log\left[\frac{1}{(\sqrt{\ln(2)} + \sqrt{\ln(2)})} \right] (142^{\mu+1} + 7) + \frac{1}{(\sqrt{\ln(2)} + \sqrt{\ln(3)})} \log\left[\frac{1}{(\sqrt{\ln(2)} + \sqrt{\ln(3)})} \right] (442^{\mu+1} + 2) + \frac{1}{(\sqrt{\ln(3)} + \sqrt{\ln(3)})} \log\left[\frac{1}{(\sqrt{\ln(3)} + \sqrt{\ln(3)})} \right] (42^{\mu+1}) \right\}$$

$$= \log[(37.6266)2^{\mu+1} + 9.0844] + \frac{[(25.94)2^{\mu+1} + 1.138]}{[(37.6266)2^{\mu+1} + 31.663]}$$

3.2. Second Generation (CD_2). $\Omega_2[3]$ represents the molecular structure of second-generation curcumin-conjugated PAMAM dendrimer in the third development stage. The respective molecular structure is depicted in Figure 8.[45]

The edges of CD_2 are partitioned into four segments by edge partition as follows.

$$E_1(\mathrm{CD}_2) = E_{13} = \{\alpha\alpha_1 \in E(\mathrm{CD}_2):\ d_\alpha(\mathrm{CD}_2) = 1 \text{ and } E(\mathrm{CD}_2) = 3\}$$

$$E_2(\mathrm{CD}_2) = E_{23} = \{\alpha\alpha_1 \in E(\mathrm{CD}_2):\ d_\alpha(\mathrm{CD}_2) = 2 \text{ and } E(\mathrm{CD}_2) = 2\}$$

$$E_3(\mathrm{CD}_2) = E_{23} = \{\alpha\alpha_1 \in E(\mathrm{CD}_2):\ d_\alpha(\mathrm{CD}_2) = 2 \text{ and } E(\mathrm{CD}_2) = 3\}$$

https://doi.org/10.1021/acsomega.4c00686
ACS Omega 2024, 9, 14558−14579

$$E_4(CD_2) = E_{33} = \{\alpha\alpha_1 \in E(CD_2): d_\alpha(CD_2) = 3 \text{ and } E(CD_2) = 3\}$$

The cardinality of the aforementioned partitions of CD_2 represented by $|E_i|$ is stated in Table 5.

Table 5. Edge Partition and Cardinality of $\Omega_2(3)$

E_i	(d_α, d_{α_1})	$\lvert E_i\rvert$
E_1	(1,2)	$11(2^{\mu+1}) + 12$
E_2	(2,2)	$14(2^{\mu+1}) + 5$
E_3	(2,3)	$44(2^{\mu+1}) + 14$
E_4	(3,3)	$4(2^{\mu+1})$

Theorem 3: The discrete adriatic indices for molecular structures of curcumin-conjugated PAMAM dendrimer of second generation $\Omega_2(3)$ where $\mu \geq 1$, with edge partitions as $|E_1| = 11(2^{\mu+1}) + 12$, $|E_2| = 14(2^{\mu+1}) + 5$, $|E_3| = 44(2^{\mu+1}) + 14$, and $|E_4| = 4(2^{\mu+1})$ are

$$1\ RLI(CD_2)(\mu) = (45.0601)2^{\mu+1} + 13.0632$$

$$2\ SLI(CD_2)(\mu) = (125.9608)2^{\mu+1} + 47.2308$$

$$3\ ISI(CD_2)(\mu) = (81.05)2^{\mu+1} + 30.8$$

$$4\ MLI(CD_2)(\mu) = (29.8862)2^{\mu+1} + 18.889$$

$$5\ MLSI(CD_2)(\mu) = (13.02299)2^{\mu+1} + 4.9431$$

$$6\ MII(CD_2)(\mu) = (14.66667)2^{\mu+1} + 10.3333$$

$$7\ MIRI(CD_2)(\mu) = (10.351)2^{\mu+1} + 6.8856$$

$$8\ MRI(CD_2)(\mu) = (22.044)2^{\mu+1} + 13.236$$

$$9\ MDI(CD_2)(\mu) = (66)2^{\mu+1} + 38$$

$$10\ MHI(CD_2)(\mu) = (9.625)2^{\mu+1} + 6.25$$

$$11\ MMRI(CD_2)(\mu) = (60.2767)2^{\mu+1} + 25.9834$$

$$12\ MMRDI(CD_2)(\mu) = (90.9443)2^{\mu+1} + 42.9310$$

$$13\ MMDI(CD_2)(\mu) = (117)2^{\mu+1} + 62$$

$$14\ MMSDI(CD_2)(\mu) = (216)2^{\mu+1} + 144.5$$

$$15\ SDDI(CD_2)(\mu) = (168)2^{\mu+1} + 80.33$$

$$16\ ISLI(CD_2)(\mu) = (44.1327)2^{\mu+1} + 21.8726$$

Proof: The proof is similar to the proof of Theorem 1.

Theorem 4: The entropy measures of CD_2 is as follows

$$1\ ENT_{RLI}(CD_2)(\mu) = \log[(45.0601)2^{\mu+1} + 13.0632] + \frac{[(6.5004)2^{\mu+1} + 2.0263]}{[(45.0601)2^{\mu+1} + 13.0632]}$$

$$2\ ENT_{SLI}(CD_2)(\mu) = \log[(125.9608)2^{\mu+1} + 47.2308] - \frac{[(30.6762)2^{\mu+1} + 9.03]}{[(125.9608)2^{\mu+1} + 47.2308]}$$

$$3\ ENT_{ISI}(CD_2)(\mu) = \log[(81.05)2^{\mu+1} + 30.8] - \frac{[(4.52)2^{\mu+1} - 0.183]}{[(81.05)2^{\mu+1} + 30.8]}$$

$$4\ ENT_{MLI}(CD_2)(\mu) = \log[(29.8862)2^{\mu+1} + 18.889] + \frac{[(6.64)2^{\mu+1} + 2.05]}{[(29.8862)2^{\mu+1} + 18.889]}$$

$$5\ ENT_{MLSI}(CD_2)(\mu) = \log[(13.0229)2^{\mu+1} + 4.943] + \frac{[(7.8318)2^{\mu+1} + 3.3126]}{[(13.0229)2^{\mu+1} + 4.943]}$$

$$6\ ENT_{MII}(CD_2)(\mu) = \log[(14.6667)2^{\mu+1} + 10.3333] - \frac{[(6.9977)2^{\mu+1} + 3.2244]}{[(14.6667)2^{\mu+1} + 10.3333]}$$

$$7\ ENT_{MIRI}(CD_2)(\mu) = \log[(10.351)2^{\mu+1} + 6.8856] + \frac{[(6.3244)2^{\mu+1} + 0.862]}{[(10.351)2^{\mu+1} + 6.8856]}$$

$$8\ ENT_{MRI}(CD_2)(\mu) = \log[(22.044)2^{\mu+1} + 13.236] + \frac{[(7.136)2^{\mu+1} + 0.687]}{[(22.044)2^{\mu+1} + 13.236]}$$

$$9\ ENT_{MDI}(CD_2)(\mu) = \log[(66)2^{\mu+1} + 38] - \frac{[(4.816)2^{\mu+1} + 20408]}{[(66)2^{\mu+1} + 38]}$$

$$10\ ENT_{MHI}(CD_2)(\mu) = \log[(9.625)2^{\mu+1} + 6.25] + \frac{[(7.903)2^{\mu+1} + 0.9415]}{[(9.625)2^{\mu+1} + 6.25]}$$

$$11\ ENT_{MMRI}(CD_2)(\mu) = \log[(60.2767)2^{\mu+1} + 25.9834] + \frac{[(4.6782)2^{\mu+1} + 2.6322]}{[(60.2767)2^{\mu+1} + 25.9834]}$$

https://doi.org/10.1021/acsomega.4c00686
ACS Omega 2024, 9, 14558−14579

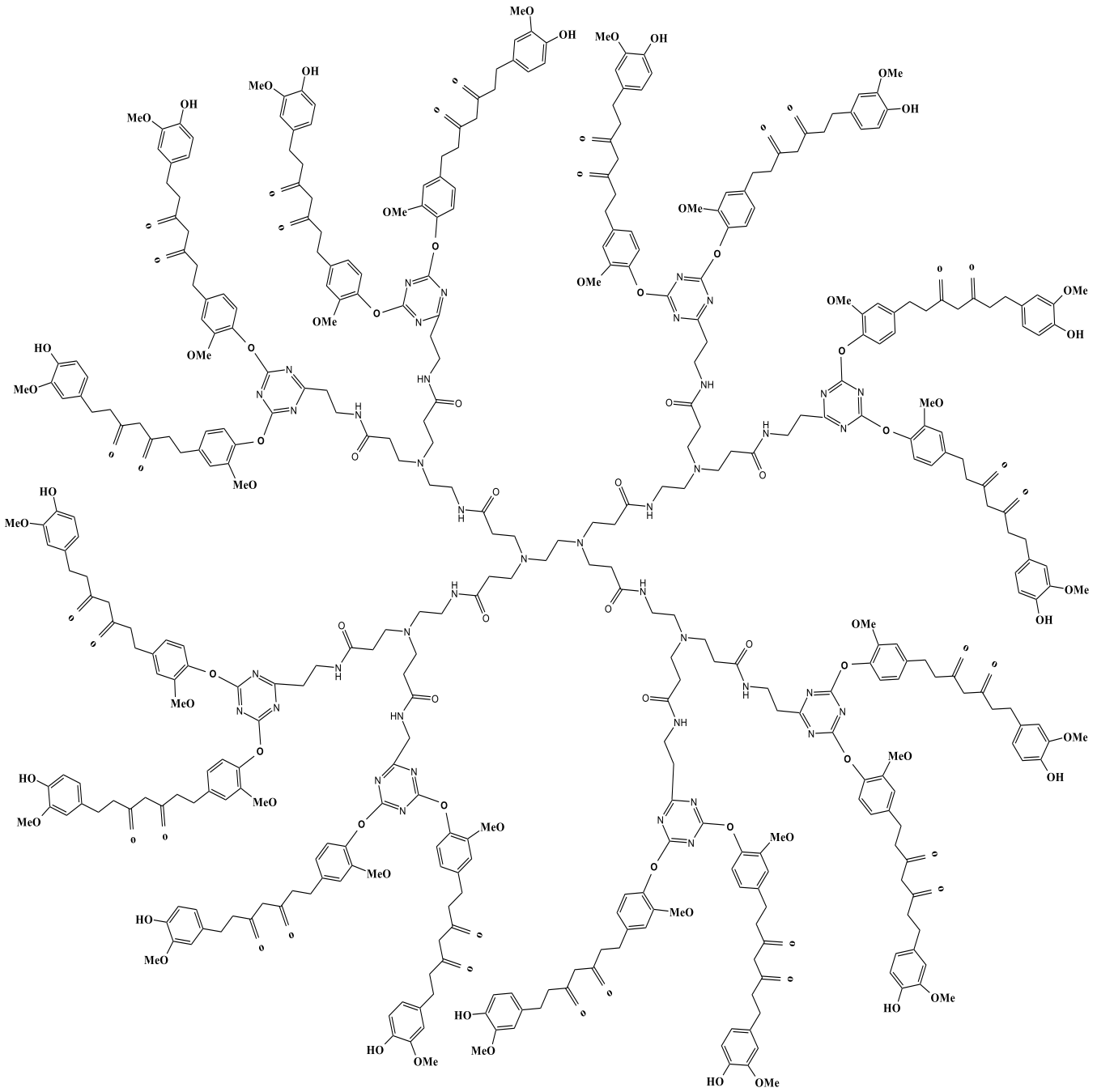

Figure 8. Second-generation PAMAM dendrimer bonded with R_1, represented as $\Omega_2(3)$.

$$12\ \mathrm{ENT}_{\mathrm{MMRDI}}(\mathrm{CD}_2)(\mu) = \log[(90.9443)2^{\mu+1} + 42.931] - \frac{[(9.2897)2^{\mu+1} + 6.4679]}{[(90.9443)2^{\mu+1} + 42.931]}$$

$$13\ \mathrm{ENT}_{\mathrm{MMDI}}(\mathrm{CD}_2)(\mu) = \log[(117)2^{\mu+1} + 62] - \frac{[(23.063)2^{\mu+1} + 6.252]}{[(117)2^{\mu+1} + 62]}$$

$$14\ \mathrm{ENT}_{\mathrm{MMSDI}}(\mathrm{CD}_2)(\mu) = \log[(216)2^{\mu+1} + 144.5] - \frac{[(103.534)2^{\mu+1} + 35.929]}{[(216)2^{\mu+1} + 144.5]}$$

$$15\ \mathrm{ENT}_{\mathrm{SDDI}}(\mathrm{CD}_2)(\mu) = \log[(168)2^{\mu+1} + 80.33] - \frac{[(56.8)2^{\mu+1} + 15.04]}{[(168)2^{\mu+1} + 80.33]}$$

https://doi.org/10.1021/acsomega.4c00686
ACS Omega 2024, 9, 14558−14579

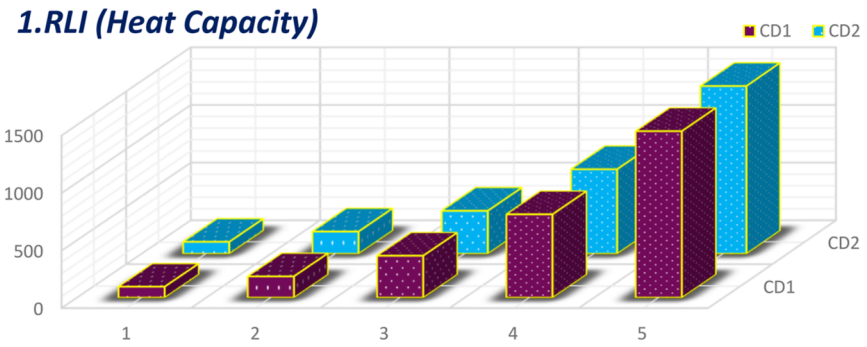

Figure 9. Comparative plot of RLI for heat capacity.

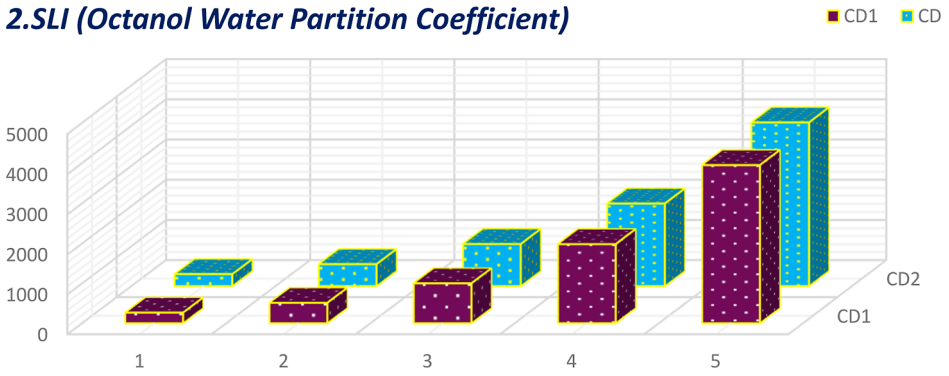

Figure 10. Comparative plot of SLI for octanol−water partition coefficient.

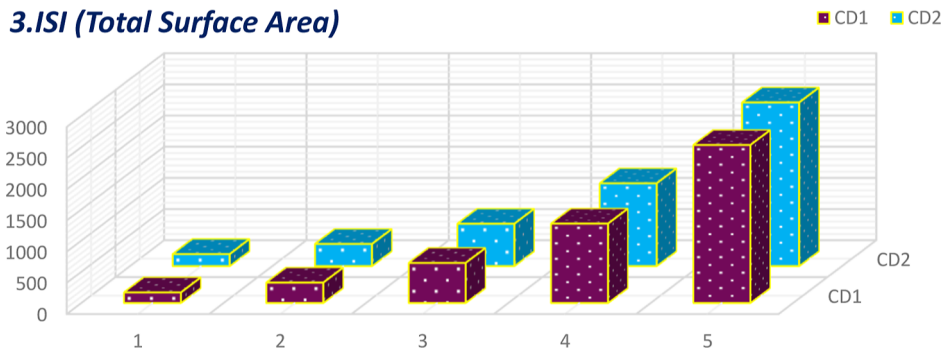

Figure 11. Comparative plot of ISI for total surface area.

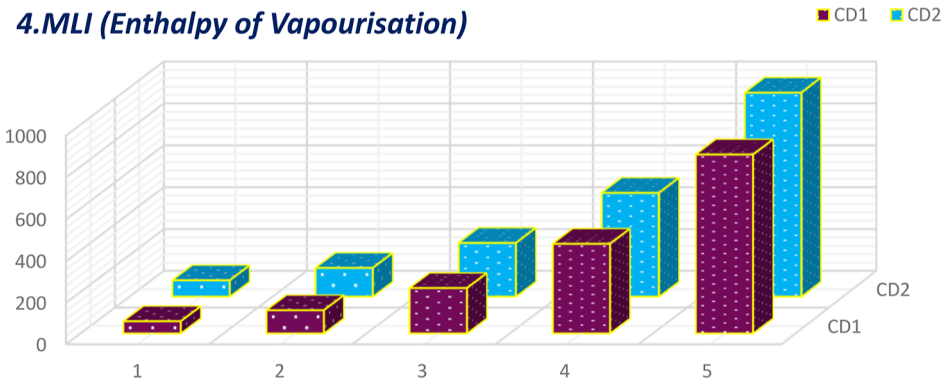

Figure 12. Comparative plot of MLI for enthalpy of vaporization.

https://doi.org/10.1021/acsomega.4c00686
ACS Omega 2024, 9, 14558−14579

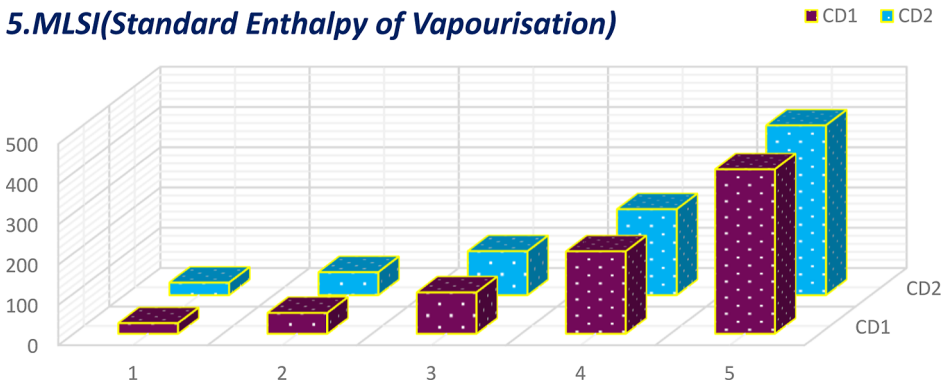

Figure 13. Comparative plot of MLSI for standard enthalpy of vaporization.

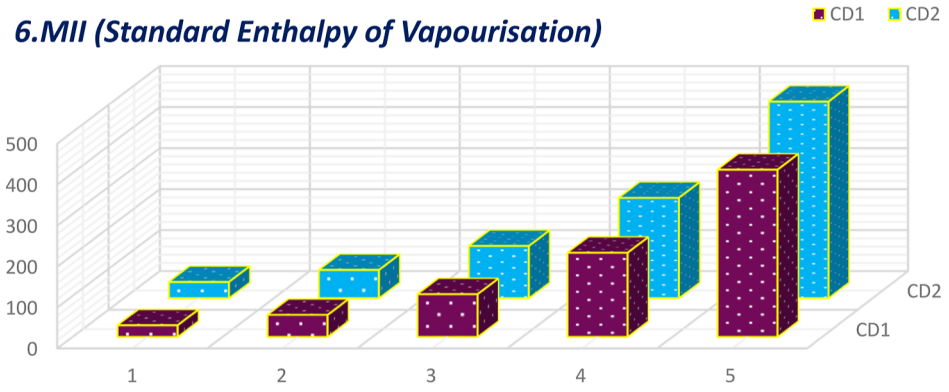

Figure 14. Comparative plot of MII for standard enthalpy of vaporization.

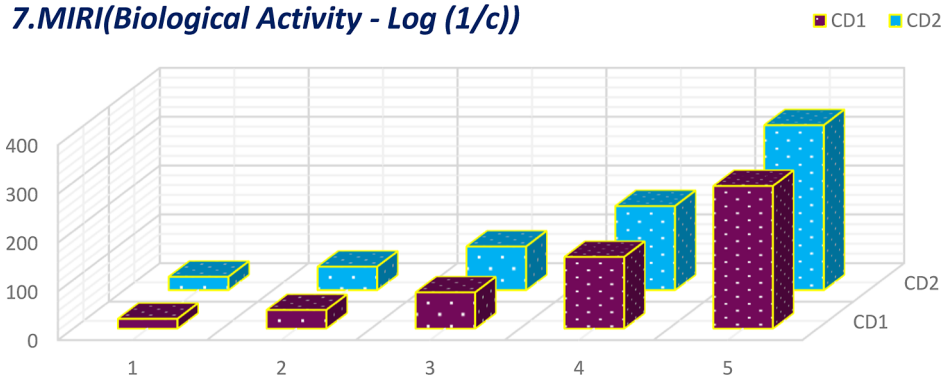

Figure 15. Comparative plot of MIRI for biological activity.

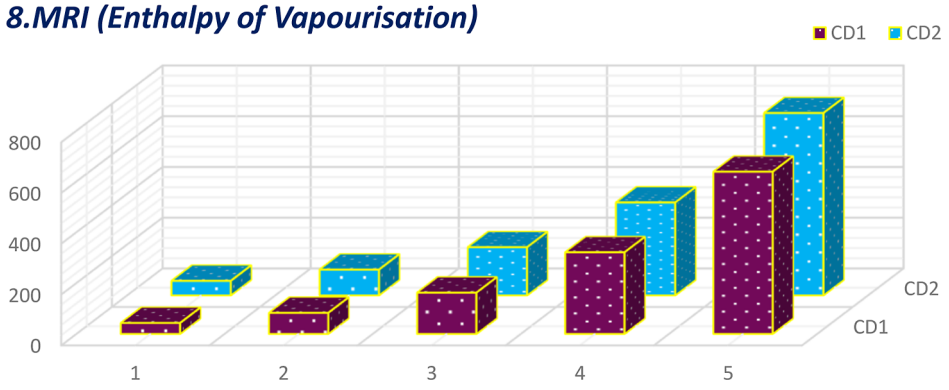

Figure 16. Comparative plot of MRI for enthalpy of vaporization.

https://doi.org/10.1021/acsomega.4c00686
ACS Omega 2024, 9, 14558−14579

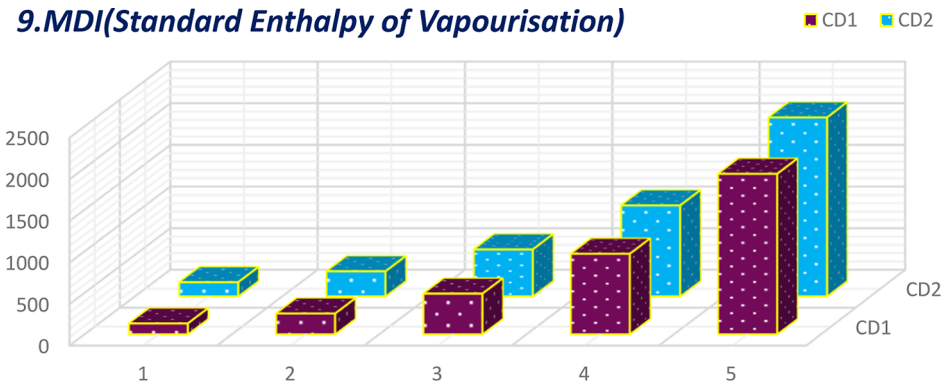

Figure 17. Comparative plot of MDI for standard enthalpy of vaporization.

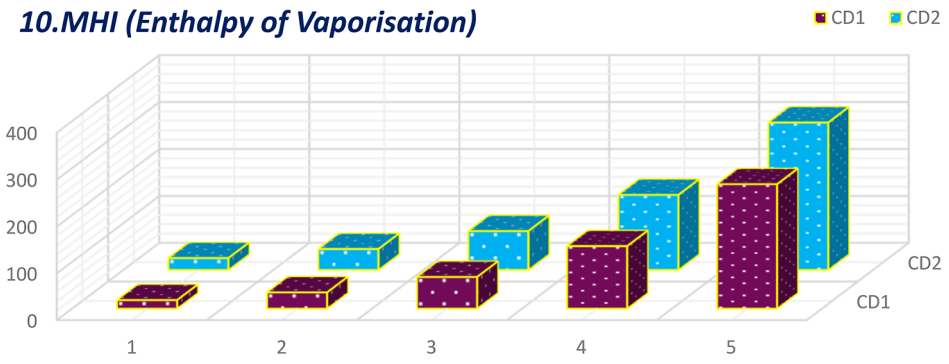

Figure 18. Comparative plot of MHI for enthalpy of vaporization.

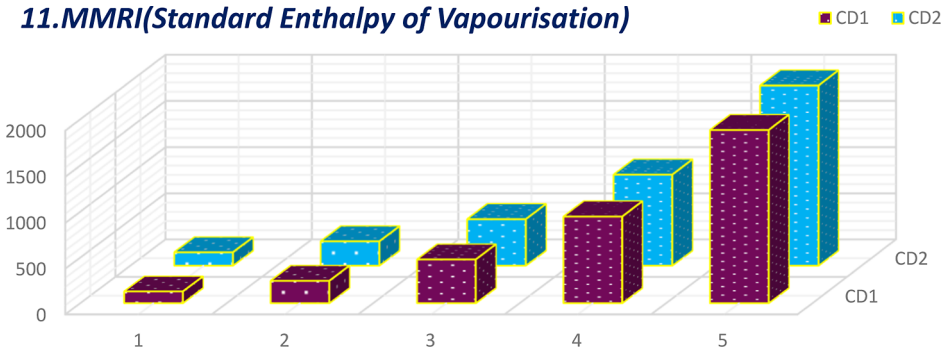

Figure 19. Comparative plot of MMRI for standard enthalpy of vaporization.

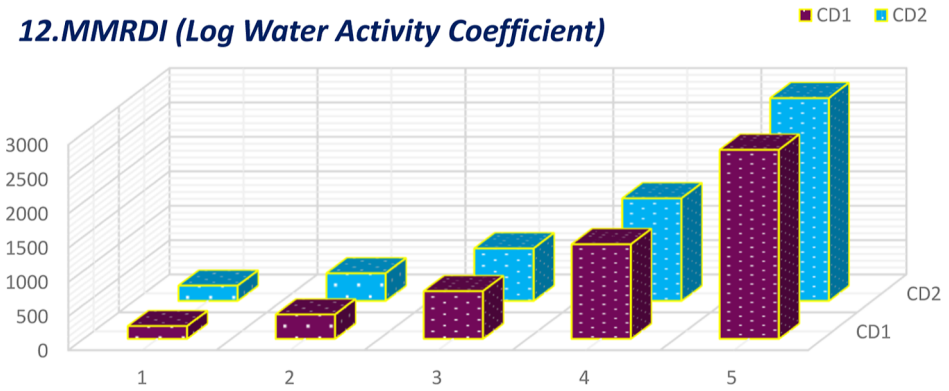

Figure 20. Comparative plot of MMRDI for Log water activity coefficient.

https://doi.org/10.1021/acsomega.4c00686
ACS Omega 2024, 9, 14558−14579

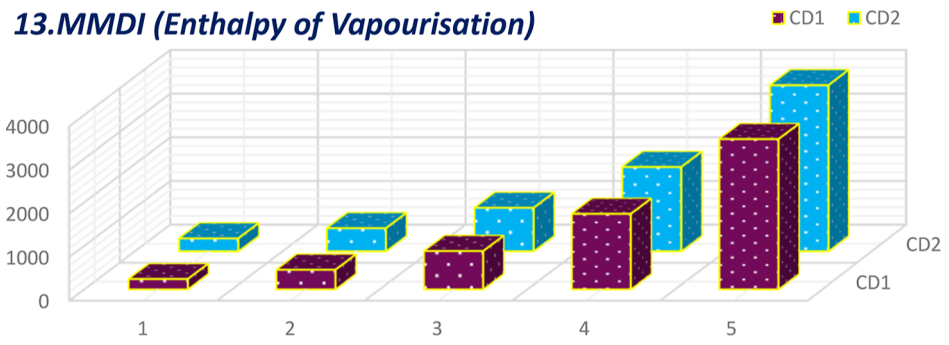

Figure 21. Comparative plot of MMDI for enthalpy of vaporization.

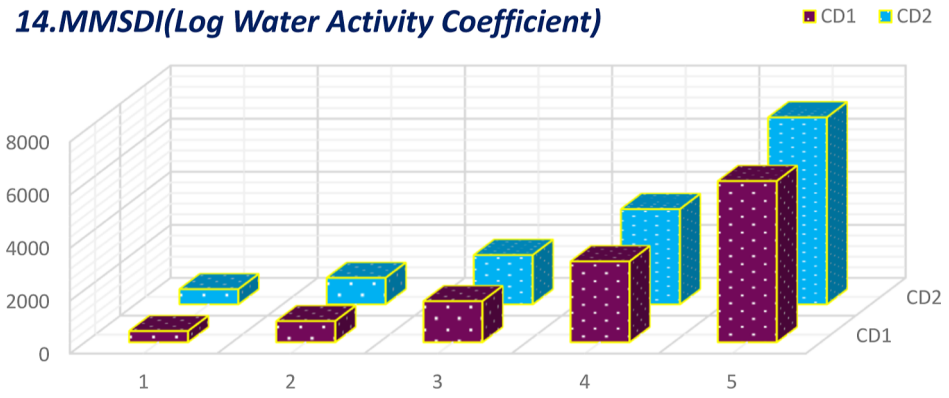

Figure 22. Comparative plot of MMSDI for Log water activity coefficient.

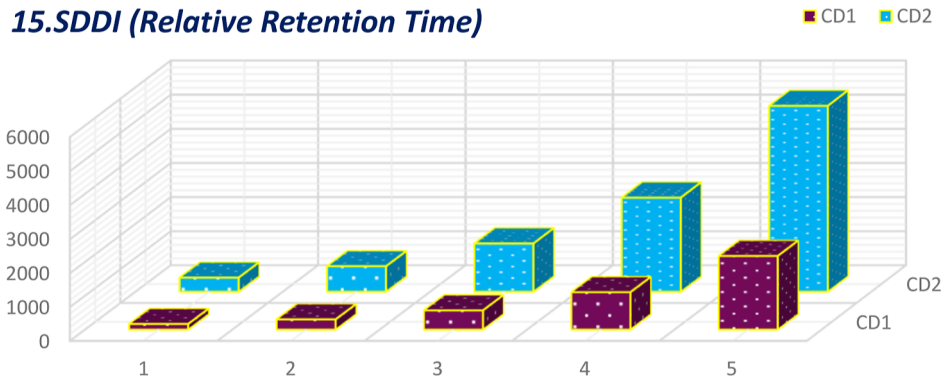

Figure 23. Comparative plot of SDDI for relative retention time.

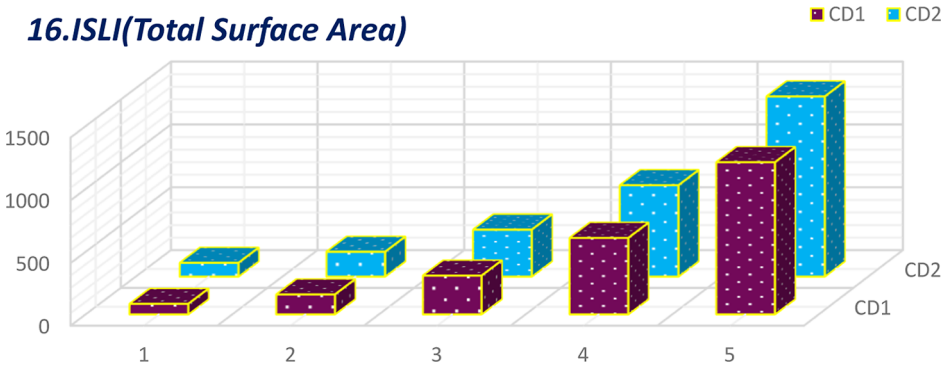

Figure 24. Comparative plot of ISLI for total surface area.

https://doi.org/10.1021/acsomega.4c00686
ACS Omega 2024, 9, 14558−14579

$$16\ \mathrm{ENT}_{\mathrm{ISLI}}(\mathrm{CD}_2)(\mu) = \log[(44.1327)2^{\mu+1} + 21.8726] + \frac{[(25.94)2^{\mu+1} + 1.138]}{[(44.1327)2^{\mu+1} + 21.8726]}$$

Proof: The proof is analogous to the proof of Theorem 2.

4. GRAPHICAL REPRESENTATION

The calculation of 16°-based TIs of the CD_1 and CD_2 structures incurred the generalized linear equation of parameter μ, the growth stage. The linear equations incurred from 16 discrete adriatic indices can be better comprehended by visualization. The numerical values obtained from the molecular descriptors for the first and second generations are shown graphically and contrasted to facilitate the understanding of the descriptors' behaviors. These comparative plots of physiochemical attributes are shown in Figures 9−24.

5. DISCUSSION

Curcumin longa is one of the most researched phytochemicals for enhancing its solubility and bioavailability. From the studies, it can be observed that curcumin bioavailability has been enhanced by Longvida and CurQfen (https://www.curqfen.net/) and PAMAM dendrimer's toxicity has been reported. But PAMAM dendrimers deliver drugs to the target better than any other means. This drug targeting would help curcumin to be delivered to the specific protein[80] which can cure many diseases that are not curable completely. This effort is meant to address the research gap theoretically as an alternative to laboratory experiments. The graphical depiction makes it clear that the physiochemical properties of the first and second generations differ in terms of total surface area, octanol−water partition coefficient, and relative retention time. Thus, the research suggests that there is a need to synthesize higher generations.

The results will facilitate the researchers for virtual screening of the molecular structure for any purpose since exploring the properties is an open problem for the chemist now. These results offer a profound insight into the topological structure of these dendrimers by predicting the physiochemical properties and comparative analysis.

The physiochemical properties of these conjugates are not widely available in globally acknowledged databases; thus, it is an open problem for the chemist to establish all of these properties through experimental results in these databases. The theoretical prediction for many widely used TIs has also not been performed by researchers so far. Prospectives involving several steps are explained in the next paragraph.

6. FUTURE PROSPECTIVES

The following phases can be used to optimize the molecular structure as a lead chemical drug: (a) using software packages like DRAGON, MathChem, GRAPHTEA, Molgen-QSPR, Generate MD, PowerMV, Molconn-Z, CODESSA, Chemical Descriptors library, AZOrange, PaDEL—Descriptors etc., various TIs/molecular descriptors required for drug design can be predicted. (b) Chemists can explore the physiochemical properties of these structures experimentally, which is still an open problem. (c) The experimental findings of CD_1 and CD_2 can be made available in international databases like EMBASE, PubChem, Drug Design Data Resource, and PubMed and used in QSPR and QSAR analyses. (d) Computer-aided drug design employing different software programs can be used for virtual screening and further optimization. (e) The true effectiveness can be finally validated through animal studies and biological lab experiments in vitro and in vivo.

7. CONCLUSIONS

In this article, the discrete adriatic indices and their entropy measures of the curcumin-conjugated PAMAM dendrimer of first and second generations are calculated and compared. Since there has never been a theoretical evaluation done previously, this work becomes distinctive and essential. The results can be very helpful in understanding the physiochemical properties of the structure which chemists have not yet fully investigated and recorded in recognized databases. Our world confronts newly identified diseases in addition to the incurable illnesses that currently exist. Therefore, the search for novel drugs is constantly needed. This process can be streamlined and made more effective by employing TIs to test a variety of substances and evaluate them in a notably short amount of time. The findings of this study support the encouraging claims regarding pharmacy engineering.

■ ASSOCIATED CONTENT

Data Availability Statement

The data sets used and/or analyzed during the current study available in this article.

Supporting Information

The Supporting Information is available free of charge at https://pubs.acs.org/doi/10.1021/acsomega.4c00686.

Synchronization of graph theory and molecular structure, bond additive TIs, and classification and nomenclature (PDF)

■ AUTHOR INFORMATION

Corresponding Author

Ammar Alsinai − *Department of Mathematics, Ibb University, Ibb 3000, Yemen;* orcid.org/0000-0002-5221-0574; Email: aliiammar1985@gmail.com

Authors

Anuradha D. S. − *Department of Mathematics, School of Advanced Sciences, Vellore Institute of Technology, Chennai 632014, India*

Konsalraj Julietraja − *Department of Mathematics, School of Engineering, Presidency University, Bengaluru 560064, India;* orcid.org/0000-0003-3108-9899

B. Jaganathan − *Department of Mathematics, School of Advanced Sciences, Vellore Institute of Technology, Chennai 632014, India*

Complete contact information is available at: https://pubs.acs.org/10.1021/acsomega.4c00686

Funding

This work was not funded by government or any private agency.

Notes

The authors declare no competing financial interest.

■ ACKNOWLEDGMENTS

The authors wish to thank the anonymous reviewers.

REFERENCES

(1) Priyadarsini, K. I. The Chemistry of Curcumin: From Extraction to Therapeutic Agent. *Molecules* **2014**, *19* (12), 20091−20112.
(2) Fadus, M. C.; Lau, C.; Bikhchandani, J.; Lynch, H. T. Curcumin: An Age-Old Anti-Inflammatory and Anti-Neoplastic Agent. *J. Tradit. Complementary Med.* **2017**, *7* (3), 339−346.
(3) Pizzo, P.; Scapin, C.; Vitadello, M.; Florean, C.; Gorza, L. Grp94 Acts as a Mediator of Curcumin-Induced Antioxidant Defence in Myogenic Cells. *J. Cell. Mol. Med.* **2010**, *14* (4), 970−981.
(4) Li, J.; Shin, G. H.; Chen, X.; Park, H. J. Modified Curcumin with Hyaluronic Acid: Combination of pro-Drug and Nano-Micelle Strategy to Address the Curcumin Challenge. *Food Res. Int.* **2015**, *69*, 202−208.
(5) Butnariu, M.; Quispe, C.; Koirala, N.; Khadka, S.; Salgado-Castillo, C. M.; Akram, M.; Anum, R.; Yeskaliyeva, B.; Cruz-Martins, N.; Martorell, M.; Kumar, M.; Vasile Bagiu, R.; Abdull Razis, A. F.; Sunusi, U.; Muhammad Kamal, R.; et al. Bioactive Effects of Curcumin in Human Immunodeficiency Virus Infection Along with the Most Effective Isolation Techniques and Type of Nanoformulations. *Int. J. Nanomed.* **2022**, *17* (August), 3619−3632.
(6) Zorofchian Moghadamtousi, S.; Abdul Kadir, H.; Hassandarvish, P.; Tajik, H.; Abubakar, S.; Zandi, K. A Review on Antibacterial, Antiviral, and Antifungal Activity of Curcumin. *BioMed Res. Int.* **2014**, *2014*, 186864.
(7) Sharma, M.; Sahu, K.; Singh, S. P.; Jain, B. Wound Healing Activity of Curcumin Conjugated to Hyaluronic Acid: In Vitro and in Vivo Evaluation. *Artif. Cells, Nanomed. Biotechnol.* **2018**, *46* (5), 1009−1017.
(8) Kalirajan, R.; Potlapati Varakumar, A. B. Activity of Phytochemical Constituents of Curcuma Longa (Turmeric) Against SARS-CoV-2 Main Protease (Covid19): Anin-Silico Approach. *Futur. J. Pharm. Sci.* **2020**, *6*, 104.
(9) Suvarna, V.; Sawant, N.; Desai, N. Curcumin-Conjugated Nanoparticles: An Approach to Target Mitochondria. *Nat. Prod.* **2024**, *14* (1), 105−117.
(10) Hemachandra Reddy, P.; Manczak, M.; Yin, X.; Grady, M. C.; Mitchell, A.; Tonk, S.; Kuruva, C. S.; Bhatti, J. S.; Kandimalla, R.; Vijayan, M.; Kumar, S.; Wang, R.; Pradeepkiran, J. A.; Ogunmokun, G.; Thamarai, K.; Quesada, K.; Reddy, A. P. Protective Effects of Indian Spice Curcumin Against Amyloid Beta in Alzheimer's Disease. *Physiol. Behav.* **2018**, *176* (10), 139−148.
(11) Giordano, A.; Tommonara, G. Curcumin and Cancer. *Nutrients* **2019**, *11* (10), 2376.
(12) Gallien, J.; Srinageshwar, B.; Gallo, K.; Holtgrefe, G.; Koneru, S.; Otero, P. S.; Bueno, C. A.; Mosher, J.; Roh, A.; Kohtz, D. S.; Swanson, D.; Sharma, A.; Dunbar, G.; Rossignol, J. Curcumin Loaded Dendrimers Specifically Reduce Viability of Glioblastoma Cell Lines. *Molecules* **2021**, *26* (19), 6050.
(13) Rafiee, Z.; Nejatian, M.; Daeihamed, M.; Jafari, S. M. Application of Curcumin-Loaded Nanocarriers for Food, Drug and Cosmetic Purposes. *Trends Food Sci. Technol.* **2019**, *88*, 445−458.
(14) Hsu, K. Y.; Ho, C. T.; Pan, M. H. The Therapeutic Potential of Curcumin and Its Related Substances in Turmeric: From Raw Material Selection to Application Strategies. *J. Food Drug Anal.* **2023**, *31* (2), 194−211.
(15) Wahlstrom, B.; Blennow, G. A Study on the Fate of Curcumin in the Rat. *Acta Pharmacol. Toxicol.* **1978**, *43* (2), 86−92.
(16) Kirmani, S. A. K. Note on Topological Indices of Hyaluronic Acid-Paclitaxel Conjugates. *Lett. Appl. NanoBioScience* **2022**, *12* (1), 4.
(17) Kirmani, S. A. K.; Ali, P. CoM-Polynomial and Topological Coindices of Hyaluronic Acid Conjugates. *Arab. J. Chem.* **2022**, *15* (7), 103911.
(18) Stohs, S. J.; Chen, O.; Ray, S. D.; Ji, J.; Bucci, L. R.; Preuss, H. G. Highly Bioavailable Forms of Curcumin and Promising Avenues for Curcumin-Based Research and Application: A Review. *Molecules* **2020**, *25* (6), 1397.
(19) Mahara, G.; Tian, C.; Xu, X.; Wang, W. Revolutionising Health Care: Exploring the Latest Advances in Medical Sciences. *J. Commun. Healthcare* **2023**, *13*, 03042.
(20) Charan, T. R.; Bhutto, M. A.; Bhutto, M. A.; Tunio, A. A.; Khuhro, G. M.; Khaskheli, S. A.; Mughal, A. A. Nanomaterials of Curcumin-Hyaluronic Acid": Their Various Methods of Formulations, Clinical and Therapeutic Applications, Present Gap, and Future Directions. *Futur. J. Pharm. Sci* **2021**, *7* (1), 126.
(21) Czyzynska-Cichon, I.; Janik-Hazuka, M.; Szafraniec-Szczęsny, J.; Jasinski, K.; Węglarz, W. P.; Zapotoczny, S.; Chlopicki, S. Low Dose Curcumin Administered in Hyaluronic Acid-Based Nanocapsules Induces Hypotensive Effect in Hypertensive Rats. *Int. J. Nanomed.* **2021**, *16*, 1377−1390.
(22) Yousefi, M.; Narmani, A.; Jafari, S. M. Dendrimers as Efficient Nanocarriers for the Protection and Delivery of Bioactive Phytochemicals. *Adv. Colloid Interface Sci.* **2020**, *278*, 102125.
(23) Sorokina, S. A.; Krasnova, I. Yu. Dendrimers: Potential Applications in Biomedicine. *INEOS Open* **2018**, *1* (2), 85−96.
(24) Sherje, A. P.; Jadhav, M.; Dravyakar, B. R.; Kadam, D. Dendrimers: A Versatile Nanocarrier for Drug Delivery and Targeting. *Int. J. Pharm.* **2018**, *548* (1), 707−720.
(25) Ghaffari, M.; Dehghan, G.; Baradaran, B.; Zarebkohan, A.; Mansoori, B.; Soleymani, J.; Ezzati Nazhad Dolatabadi, J.; Hamblin, M. R. Co-Delivery of Curcumin and Bcl-2 SiRNA by PAMAM Dendrimers for Enhancement of the Therapeutic Efficacy in HeLa Cancer Cells. *Colloids Surf., B* **2020**, *188*, 110762.
(26) Abbasi, E.; Aval, S. F.; Akbarzadeh, A.; Milani, M.; Nasrabadi, H. T.; Joo, S. W.; Hanifehpour, Y.; Nejati-Koshki, K.; Pashaei-Asl, R. Dendrimers: Synthesis, Applications, and Properties. *Nanoscale Res. Lett.* **2014**, *9* (1), 247.
(27) Tomalia, D. A.; Baker, H.; Dewald, J.; Hall, M.; Kallos, G.; Martin, S.; Roeck, S. New Class of Polymers: Starburst-Dendritic Macromolecules. *Polym. J.. 1385*, pp 117−132. .
(28) Kwon, S.; Bae, H.; Jo, J.; Yoon, S. Comprehensive Ensemble in QSAR Prediction for Drug Discovery. *BMC Bioinf.* **2019**, *20* (1), 521.
(29) Sahu, S. K.; Ojha, K. K. Applications of QSAR Study in Drug Design of Tubulin Binding Inhibitors. *J. Biomol. Struct. Dyn.* **2023**, 1−16.
(30) Murugan, G.; Julietraja, K.; Alsinai, A. Computation of Neighborhood M-Polynomial of Cycloparaphenylene and Its Variants. *ACS Omega* **2023**, *8*, 49165−49174.
(31) Zaman, S.; Ullah, A.; Shafaqat, A. Structural Modeling and Topological Characterization of Three Kinds of Dendrimer Networks. *Eur. Phys. J. E Soft Matter* **2023**, *46* (5), 36.
(32) Ullah, A.; Zaman, S.; Hamraz, A.; Muzammal, M. On the Construction of Some Bioconjugate Networks and Their Structural Modeling via Irregularity Topological Indices. *Eur. Phys. J. E* **2023**, *46* (8), 72.
(33) Zaman, S.; Jalani, M.; Ullah, A.; Ali, M.; Shahzadi, T. On the Topological Descriptors and Structural Analysis of Cerium Oxide Nanostructures. *Chem. Pap.* **2023**, *77* (5), 2917−2922.
(34) Zaman, S.; Jalani, M.; Ullah, A.; Saeedi, G. Structural Analysis and Topological Characterization of Sudoku Nanosheet. *J. Math.* **2022**, *2022*, 5915740.
(35) Liu, P.; Long, W. Current Mathematical Methods Used in QSAR/QSPR Studies. *Int. J. Mol. Sci.* **2009**, *10* (5), 1978−1998.
(36) Shanmukha, M. C.; Basavarajappa, N. S.; Shilpa, K. C.; Usha, A. Degree-Based Topological Indices on Anticancer Drugs with QSPR Analysis. *Heliyon* **2020**, *6* (6), No. e04235.
(37) Sardar, M. S.; Ali, M. A.; Farahani, M. R.; Alaeiyan, M.; Cancan, M.; Campus, Z. Topological Indices and QSPR/QSAR Analysis of Some Drugs Being Investigated for the Treatment of Headaches. *Eur. Chem. Bull.* **2023**, *12* (5), 69−83.
(38) Kirmani, S. A. K.; Ali, P.; Azam, F. Topological Indices and QSPR/QSAR Analysis of Some Antiviral Drugs Being Investigated for the Treatment of COVID-19 Patients. *Int. J. Quantum Chem.* **2021**, *121* (9), 1−22.
(39) Gnanaraj, L. R. M.; Ganesan, D.; Siddiqui, M. K. Topological Indices and QSPR Analysis of NSAID Drugs. *Polycyclic Aromat. Compd.* **2023**, *43* (10), 9479−9495.
(40) Zhang, X.; Saif, M. J.; Idrees, N.; Kanwal, S.; Parveen, S.; Saeed, F. QSPR Analysis of Drugs for Treatment of Schizophrenia Using Topological Indices. *ACS Omega* **2023**, *8* (44), 41417−41426.

https://doi.org/10.1021/acsomega.4c00686
ACS Omega 2024, 9, 14558−14579

(41) Verma, J.; Khedkar, V.; Coutinho, E. 3D-QSAR in Drug Design - A Review. *Curr. Top. Med. Chem.* **2010**, *10* (1), 95−115.
(42) Abdel-Ilah, L.; Veljović, E.; Gurbeta, L.; Badnjević, A. Applications of QSAR Study in. Drug Design. *Int. J. Eng. Res. Technol.* **2017**, *6* (06), 582−587.
(43) Vaughn, A. R.; Branum, A.; Sivamani, R. K. Effects of Turmeric (Curcuma Longa) on Skin Health: A Systematic Review of the Clinical Evidence. *Phytother Res.* **2016**, *30*, 1243−1264.
(44) Dodangeh, M.; Gharanjig, K.; Tang, R. C.; Grabchev, I. Functionalization of PAMAM Dendrimers with Curcumin: Synthesis, Characterization, Fluorescent Improvement and Application on PET Polymer. *Dyes Pigm.* **2020**, *174*, 108081.
(45) Dodangeh, M.; Grabchev, I.; Gharanjig, K.; Staneva, D.; Tang, R. C.; Sheridan, M. Modified PAMAM Dendrimers as a Matrix for the Photostabilization of Curcumin. *New J. Chem.* **2020**, *44* (39), 17112−17121.
(46) Zanni, R.; Galvez-Llompart, M.; García-Domenech, R.; Galvez, J. Latest Advances in Molecular Topology Applications for Drug Discovery. *Expert Opin. Drug Discovery* **2015**, *10* (9), 945−957.
(47) Estrada, E.; Uriarte, E. Recent Advances on the Role of Topological Indices in Drug Discovery Research. *Curr. Med. Chem.* **2001**, *8* (13), 1573−1588. http://www.cas.org/cgiweb-
(48) Sathyanarayanan, A. D.; Jaganathan, B. Topological Properties of Boron Triangular Sheet for Robotic Finger Flex Motion through Indices. *AIP Conf. Proc.* **2023**, *2946* (1), 020013.
(49) Ds, A.; Jaganathan, B. PhysioChemical Properties of Benzophenone and Curcumin Conjugated PAMAM Dendrimers Using Topological Indices. *Polycycl. Aromat. Comp.* **2023**, 1−23.
(50) Vukicevic, D.; Gasperov, M. Bond Additive Modeling 1. Adriatic Indices. *Croat. Chem. Acta* **2010**, *83* (3), 243−260.
(51) Cao, J.; Zhang, H.; Wang, Y.; Yang, J.; Jiang, F. Investigation on the Interaction Behavior between Curcumin and PAMAM Dendrimer by Spectral and Docking Studies. *Spectrochim. Acta, Part A* **2013**, *108*, 251−255.
(52) Fernandes, G.; Pandey, A.; Kulkarni, S.; Mutalik, S. P.; Nikam, A. N.; Seetharam, R. N.; Kulkarni, S. S.; Mutalik, S. Supramolecular dendrimers based novel platforms for effective oral delivery of therapeutic moieties. *J. Drug Deliv. Sci. Technol.* **2021**, *64*, 102647.
(53) Tripathi, P. K.; Gupta, S.; Rai, S.; Shrivatava, A.; Tripathi, S.; Singh, S.; Khopade, A. J.; Kesharwani, P. Curcumin Loaded Poly (Amidoamine) Dendrimer-Plamitic Acid Core-Shell Nanoparticles as Anti-Stress Therapeutics. *Drug Dev. Ind. Pharm.* **2020**, *46* (3), 412−426.
(54) Todeschini, R.; Consonni, V. *Handbook of Molecular Descriptors*; MAnnhold, R., Kubinyi, H. H. T., Eds.; Wiley VCH, 2008.
(55) Baby, A.; Julietraja, K.; Xavier, D. A. On Molecular Structural Characterization of Cyclen Cored Dendrimers. *Polycycl. Aromat. Comp.* **2024**, *44*, 707−729.
(56) Rahul, M. P.; Clement, J.; Singh Junias, J.; Arockiaraj, M.; Balasubramanian, K. Degree-Based Entropies of Graphene, Graphyne and Graphdiyne Using Shannon's Approach. *J. Mol. Struct.* **2022**, *1260*, 132797.
(57) Julietraja, K.; Venugopal, P. Computation of Degree-Based Topological Descriptors Using M-Polynomial for Coronoid Systems. *Polycyclic Aromat. Compd.* **2022**, *42* (4), 1770−1793.
(58) Julietraja, K.; Venugopal, P.; Prabhu, S.; S, D.; Siddiqui, M. K. Molecular Structural Descriptors of Donut Benzenoid Systems. *Polycyclic Aromat. Compd.* **2022**, *42* (7), 4146−4172.
(59) Julietraja, K.; Alsinai, A.; Alameri, A. Theoretical Analysis of Superphenalene Using Different Kinds of VDB Indices. *J. Chem.* **2022**, *2022*, 5683644.
(60) Julietraja, K.; Venugopal, P.; Prabhu, S.; Liu, J. B. M-Polynomial and Degree-Based Molecular Descriptors of Certain Classes of Benzenoid Systems. *Polycyclic Aromat. Compd.* **2022**, *42* (6), 3450−3477.
(61) Chu, Y. M.; Julietraja, K.; Venugopal, P.; Siddiqui, M. K.; Prabhu, S. Degree- and Irregularity-Based Molecular Descriptors for Benzenoid Systems. *Eur. Phys. J. Plus* **2021**, *136* (1), 78.
(62) Konsalraj, J.; Padmanabhan, V.; Perumal, C. Topological Analysis of PAHs Using Irregularity Based Indices. *Biointerface Res. Appl. Chem.* **2022**, *12* (3), 2970−2987.
(63) Zhao, W.; Julietraja, K.; Venugopal, P.; Zhang, X. VDB Entropy Measures and Irregularity-Based Indices for the Rectangular Kekulene System. *J. Math.* **2021**, *2021*, 7404529.
(64) Yang, J.; Konsalraj, J.; Raja S, A. A. Neighbourhood Sum Degree-Based Indices and Entropy Measures for Certain Family of Graphene Molecules. *Molecules* **2022**, *28* (1), 168.
(65) Tharmalingam, G.; Ponnusamy, K.; Govindhan, M.; Konsalraj, J. On Certain Degree Based and Bond Additive Molecular Descriptors of Hexabenzocorenene. *Biointerface Res. Appl. Chem.* **2023**, *13* (5), 495.
(66) Sharma, K.; Bhat, V. K.; Sharma, S. K. On Degree-Based Topological Indices of Carbon Nanocones. *ACS Omega* **2022**, *7* (49), 45562−45573.
(67) Konsalraj, J.; Padmanabhan, V.; Perumal, C. Vdb Analysis for Zeolites Lta Structures. *Biointerface Res. Appl. Chem.* **2022**, *12* (5), 6960−6977.
(68) Adnan, M.; Bokhary, S. A. U. H.; Abbas, G.; Iqbal, T. Degree-Based Topological Indices and QSPR Analysis of Antituberculosis Drugs. *J. Chem.* **2022**, *2022*, 5748626.
(69) Parveen, S.; Awan, N. U. H.; Farooq, F. B.; Fanja, R.; Anjum, Q. U. A. Topological Indices of Novel Drugs Used in Autoimmune Disease Vitiligo Treatment and Its QSPR Modeling. *BioMed Res. Int.* **2022**, *2022*, 6045066.
(70) Hussain, S.; Afzal, F.; Afzal, D.; Thapa, D. K. The Study about Relationship of Direct Form of Topological Indices via M-Polynomial and Computational Analysis of Dexamethasone. *J. Chem.* **2022**, *2022*, 4912143.
(71) Wang, W.; Naeem, M.; Rauf, A.; Riasat, A.; Aslam, A.; Anoh Yannick, K. On Analysis of Banhatti Indices for Hyaluronic Acid Curcumin and Hydroxychloroquine. *J. Chem.* **2021**, *2021*, 7468857.
(72) Gao, W.; Siddiqui, M. K.; Rehman, N. A.; Muhammad, M. H. Topological Characterization of Dendrimer, Benzenoid, and Nanocone. *Z. Naturforsch., C: J. Biosci.* **2018**, *74* (1−2), 35−43.
(73) Xavier, D. A.; Julietraja, K.; Nair A, T.; Baby, A.; Julietraja, K.; Xavier, D. A.; Alsinai, A.; Alameri, A.; Yang, J.; Konsalraj, J.; Raja S, A. A.; Saravanan, B.; Prabhu, S.; Arulperumjothi, M.; Julietraja, K.; Siddiqui, M. K.; Xavier, D. A.; Akhila, S.; Alsinai, A.; Julietraja, K.; Ahmed, H.; Raja, A. A.; Varghese, E. S.; Zhao, W.; Julietraja, K.; Venugopal, P.; Zhang, X.; Prabhu, S.; Arulmozhi, A. K.; Siddiqui, M. K.; Liu, J. B.; K, J.; P, V.; S, P.; S, D.; Siddiqui, M. K.; Chu, Y. M.; Julietraja, K.; Venugopal, P.; Siddiqui, M. K.; Prabhu, S. Computation of Degree-Based Topological Descriptors Using M-Polynomial for Coronoid Systems. *Polycyclic Aromat. Compd.* **2022**, *42* (0), 1770−1793.
(74) Balasubramaniyan, D.; Chidambaram, N. On Some Neighbourhood Degree-Based Topological Indices with QSPR Analysis of Asthma Drugs. *Eur. Phys. J. Plus* **2023**, *138*, 823.
(75) Ali, P.; Kirmani, S. A. K.; Al Rugaie, O.; Azam, F. Degree-Based Topological Indices and Polynomials of Hyaluronic Acid-Curcumin Conjugates. *Saudi Pharmaceut. J.* **2020**, *28* (9), 1093−1100.
(76) Sabirov, D. S.; Shepelevich, I. S. Information Entropy in Chemistry: An Overview. *Entropy* **2021**, *23* (10), 1240.
(77) Mowshowitz, A.; Dehmer, M. Entropy and the Complexity of Graphs Revisited. *Entropy* **2012**, *14* (3), 559−570.
(78) Estrada, E.; de la Peña, J. A.; Hatano, N. Walk Entropies in Graphs. *Lin. Algebra Appl.* **2014**, *443*, 235−244.
(79) Julietraja, K.; Venugopal, P.; Prabhu, S.; Arulmozhi, A. K.; Siddiqui, M. K. Structural Analysis of Three Types of PAHs Using Entropy Measures. *Polycyclic Aromat. Compd.* **2022**, *42* (7), 4101−4131.
(80) Wang, J.; Li, B.; Qiu, L.; Qiao, X.; Yang, H. Dendrimer-Based Drug Delivery Systems: History, Challenges, and Latest Developments. *J. Biol. Eng.* **2022**, *16* (1), 18.

https://doi.org/10.1021/acsomega.4c00686
ACS Omega 2024, 9, 14558−14579